References

[1] M.A. Marra, S.J. Jones, C.R. Astell, R.A. Holt, A. Brooks-Wilson, Y.S. Butterfield, J. Khattra, J.K. Asano, S.A. Barber, S.Y. Chan, A. Cloutier, S.M. Coughlin, D. Freeman, N. Girn, O.L. Griffith, S.R. Leach, M. Mayo, H. McDonald, S.B. Montgomery, P.K. Pandoh, A.S. Petrescu, A.G. Robertson, J.E. Schein, A. Siddiqui, D.E. Smailus, J.M. Stott, G.S. Yang, F. Plummer, A. Andonov, H. Artsob, N. Bastien, K. Bernard, T.F. Booth, D. Bowness, M. Czub, M. Drebot, L. Fernando, R. Flick, M. Garbutt, M. Gray, A. Grolla, S. Jones, H. Feldmann, A. Meyers, A. Kabani, Y. Li, S. Normand, U. Stroher, G.A. Tipples, S. Tyler, R. Vogrig, D. Ward, B. Watson, R.C. Brunham, M. Krajden, M. Petric, D.M. Skowronski, C. Upton, R.L. Roper, The genome sequence of the SARS-associated coronavirus, Science 300 (2003) 1399–1404.

[2] P.A. Rota, M.S. Oberste, S.S. Monroe, W.A. Nix, R. Campagnoli, J.P. Icenogle, S. Penaranda, B. Bankamp, K. Maher, M.H. Chen, S. Tong, A. Tamin, L. Lowe, M. Frace, J.L. DeRisi, Q. Chen, D. Wang, D.D. Erdman, T.C. Peret, C. Burns, T.G. Ksiazek, P.E. Rollin, A. Sanchez, S. Liffick, B. Holloway, J. Limor, K. McCaustland, M. Olsen-Rasmussen, R. Fouchier, S. Gunther, A.D. Osterhaus, C. Drosten, M.A. Pallansch, L.J. Anderson, W.J. Bellini, Characterization of a novel coronavirus associated with severe acute respiratory syndrome, Science 300 (2003) 1394–1399.

[3] T. Mizutani, S. Fukushi, M. Saijo, I. Kurane, S. Morikawa, Phosphorylation of p38 MAPK and its downstream targets in SARS coronavirus-infected cells, Biochem. Biophys. Res. Commun. 319 (2004) 1228–1234.

[4] T. Mizutani, S. Fukushi, M. Saijo, I. Kurane, S. Morikawa, Importance of Akt signaling pathway for apoptosis in SARS-CoV-infected Vero E6 cells, Virology 327 (2004) 169–174.

[5] T. Mizutani, S. Fukushi, M. Murakami, T. Hirano, M. Saijo, I. Kurane, S. Morikawa, Tyrosine dephosphorylation of STAT3 in SARS coronavirus-infected Vero E6 cells, FEBS Lett. 577 (2004) 187–192.

[6] T. Mizutani, S. Fukushi, M. Saijo, I. Kurane, S. Morikawa, Regulation of p90RSK phosphorylation by SARS-CoV infection in Vero E6 cells, FEBS Lett. 580 (2006) 1417–1424.

[7] T. Mizutani, S. Fukushi, M. Saijo, I. Kurane, S. Morikawa, JNK and PI3k/Akt signaling pathways are required for establishing persistent SARS-CoV infection in Vero E6 cells, Biochem. Biophys. Acta 1741 (2005) 4–10.

[8] P.K. Chan, K.F. To, A.W. Lo, J.L. Cheung, I. Chu, F.W. Au, J.H. Tong, J.S. Tam, J.J.J. Sung, H.K. Ng, Persistent infection of SARS coronavirus in colonic cells in vitro, J. Med. Virol. 74 (2004) 1–7.

[9] G. Palacios, O. Jabado, N. Renwick, T. Briese, W.I. Lipkin, Severe acute respiratory syndrome coronavirus persistence in Vero cells, Chin. Med. J. (Engl.) 118 (2005) 451–459.

[10] M. Yamate, M. Yamashita, T. Goto, S. Tsuji, Y.G. Li, J. Warachit, M. Yunoki, K. Ikuta, Establishment of Vero E6 cell clones persistently infected with severe acute respiratory syndrome coronavirus, Microbes Infect. 7 (2005) 1530–1540.

[11] K. Ishii, H. Hasegawa, N. Nagata, M. Mizutani, S. Morikawa, T. Suzuki, F. Taguchi, M. Tashiro, T. Takemori, T. Miyamura, Y. Tsunetsugu-Yokota, Induction of protective immunity against severe acute respiratory syndrome coronavirus (SARS-CoV) infection using highly attenuated recombinant vaccinia virus DIs, Virology (in press).

[12] E. Everitt, C. Wohlfart, Spectrophotometric quantitation of anchorage-dependent cell numbers using extraction of naphthol blue-black-stained cellular protein, Anal. Biochem. 162 (1987) 122–129.

[13] T. Mizutani, S. Fukushi, D. Iizuka, O. Inanami, M. Kuwabara, H. Takashima, H. Yanagawa, M. Saijo, I. Kurane, S. Morikawa, Inhibition of cell proliferation by SARS-CoV infection in Vero E6 cells, FEMS Immunol. Med. Microbiol. 46 (2006) 236–243.

[14] R. Kim, Unknotting the roles of Bcl-2 and Bcl-xL in cell death, Biochem. Biophys. Res. Commun. 333 (2005) 336–343.

[15] M. Surjit, B. Liu, S. Jameel, V.T. Chow, S.K. Lal, The SARS coronavirus nucleocapsid protein induces actin reorganization and apoptosis in COS-1 cells in the absence of growth factors, Biochem. J. 383 (2004) 13–18.

Available online at www.sciencedirect.com
SCIENCE DIRECT
Virology 351 (2006) 381–392
VIROLOGY
www.elsevier.com/locate/yviro

Production of infectious hepatitis C virus particles in three-dimensional cultures of the cell line carrying the genome-length dicistronic viral RNA of genotype 1b

Kyoko Murakami [a], Koji Ishii [a], Yousuke Ishihara [b], Sayaka Yoshizaki [a], Keiko Tanaka [c], Yasufumi Gotoh [d,e], Hideki Aizaki [a], Michinori Kohara [f], Hiroshi Yoshioka [g], Yuichi Mori [g], Noboru Manabe [d], Ikuo Shoji [a], Tetsutaro Sata [c], Ralf Bartenschlager [h], Yoshiharu Matsuura [i], Tatsuo Miyamura [a], Tetsuro Suzuki [a,*]

[a] *Department of Virology II, National Institute of Infectious Diseases, 1-23-1 Toyama, Shinjuku-ku, Tokyo 162-8640, Japan*
[b] *Hanaichi Ultrastructure Research Institute, Okazaki, Aichi 444-0076, Japan*
[c] *Department of Pathology, National Institute of Infectious Diseases, Shinjuku, Tokyo 162-8640, Japan*
[d] *Research Unit for Animal Life Sciences, Animal Resource Science Center, The University of Tokyo, Iwama, Ibaraki 319-0206, Japan*
[e] *Unit of Anatomy and Cell Biology, Department of Animal Sciences, Kyoto University, Kyoto 606-8502, Japan*
[f] *Department of Microbiology and Cell Biology, Tokyo Metropolitan Institute of Medical Science, Bunkyo-ku, Tokyo 113-8613, Japan*
[g] *Mebiol Inc., Hiratsuka, Kanagawa 254-0075, Japan*
[h] *Department of Molecular Virology, Hygiene Institute, University Heidelberg, Im Neuenheimer Feld 345, D-69120 Heidelberg, Germany*
[i] *Department of Molecular Virology, Research Institute for Microbial Diseases, Osaka University, Suita, Osaka 565-0871, Japan*

Received 5 January 2006; returned to author with revision 23 January 2006; accepted 24 March 2006
Available online 6 May 2006

Abstract

We show that a dicistronic hepatitis C virus (HCV) genome of genotype 1b supports the production and secretion of infectious HCV particles in two independent three-dimensional (3D) culture systems, the radial-flow bioreactor and the thermoreversible gelation polymer (TGP), but not in monolayer cultures. Immunoreactive enveloped particles, which are 50–60 nm in diameter and are surrounded by membrane-like structures, are observed in the culture medium as well as at the endoplasmic reticulum membranes and in dilated cytoplasmic cisternae in spheroids of Huh-7 cells. Infection of HCV particles is neutralized by anti-E2 antibody or patient sera that interfere with E2 binding to human cells. Finally, the utility of the 3D-TGP culture system for the evaluation of antiviral drugs is shown. We conclude that the replicon-based 3D culture system allows the production of infectious HCV particles. This system is a valuable tool in studies of HCV morphogenesis in a natural host cell environment.
© 2006 Elsevier Inc. All rights reserved.

Keywords: Hepatitis C virus; Replication; Three-dimensional culture; Virus particle

Introduction

Infection with hepatitis C virus (HCV) currently represents a major medical and socioeconomic problem. HCV is a main causative agent of chronic hepatitis, cirrhosis, and hepatocellular carcinoma, and there are an estimated 170 million HCV carriers worldwide (Choo et al., 1989). The standard treatments for HCV infection are interferon alpha (IFN-α) in combination with ribavirin (RBV) or, more recently, a polyethylene glycol-modified form of IFN-α; however, sustained response is seen in only ~50% of treated patients (Davis et al., 2003; Manns et al., 2001). Further development of new anti-HCV drugs and vaccines has been obstructed by the lack of either a small animal model or a robust cell culture system capable of supporting viral replication and the production of infectious progeny.

HCV is a small enveloped RNA virus belonging to the family Flaviviridae and harboring a single-stranded RNA genome with

* Corresponding author. Fax: +81 3 5285 1161.
E-mail address: tesuzuki@nih.go.jp (T. Suzuki).

0042-6822/$ - see front matter © 2006 Elsevier Inc. All rights reserved.
doi:10.1016/j.virol.2006.03.038

positive polarity. A precursor polyprotein of ~3000 amino acids (aa) is encoded by a large open reading frame. This polyprotein is cleaved by cellular and viral proteases to give rise to a series of structural and nonstructural proteins (Choo et al., 1991; Grakoui et al., 1993; Hijikata et al., 1991). The establishment of selectable dicistronic HCV RNAs that are capable of autonomous replication in human hepatoma Huh-7 cells was a significant breakthrough in HCV research (Blight et al., 2000; Lohmann et al., 1999) and has provided an important tool for the study of HCV replication mechanisms and for screening antiviral drugs (Frese et al., 2001; Guo et al., 2001). This replicon system was first developed to replicate only viral subgenomic RNAs but has been further expanded to enable the replication of genome-length dicistronic RNAs (Ikeda et al., 2002; Pietschmann et al., 2002). Although the viral genome replicates and all HCV proteins are properly processed in this system, virus particle production has not yet been achieved. A number of researchers (Date et al., 2004; Kato et al., 2001, 2003) have developed an HCV genotype 2a replicon (JFH-1) that efficiently replicates in a variety of human cells. Recently, it has been demonstrated that the full-length JFH-1 genome or a chimeric genome using JFH-1 and J6, a related genotype 2a strain, produces infectious particles in cell cultures (Lindenbach et al., 2005; Wakita et al., 2005; Zhong et al., 2005). More recently, production of infectious genotype 1a virus (Hutchinson strain) using similar experimental systems has been described (Yi et al., 2006). These complete HCV culture systems produce robust levels of infectious virus and provides a powerful tool for HCV research. However, to date their applications have not been extended to constructs based on strains of genotype 1b, which is highly prevalent worldwide.

We previously demonstrated that differentiated human hepatoma FLC4 cells transfected with in vitro transcribed HCV genomic RNA can produce and secrete infectious particles in three-dimensional (3D) radial-flow bioreactor (RFB) culture (Aizaki et al., 2003). This RFB system was initially aimed to develop artificial liver tissue, and the bioreactor column consists of a vertically extended cylindrical matrix through which liquid medium flows continuously from the periphery toward the center of the reactor (Kawada et al., 1998). In RFB culture, human hepatocellular carcinoma-derived cells can grow spherically or cubically, and they retain liver functions such as albumin synthesis (Kawada et al., 1998; Matsuura et al., 1998) and drug-metabolizing activity mediated by cytochrome P450 3A4 (Iwahori et al., 2003).

In the present study, two kinds of 3D culture techniques, the RFB and the thermoreversible gelation polymer (TGP), were used for the production and secretion of infectious HCV particles by using a dicistronic HCV genome derived from genotype 1b. We also demonstrate that these 3D culture systems are useful for evaluating anti-HCV drugs.

Results

Secretion of HCV-LPs from RCYM1 carrying genome-length dicistronic HCV RNA cultured in RFB culture

We first assessed the replicative capacity of selectable genome-length HCV RNAs in FLC4 cells. However, no G418-resistant colonies were observed, indicating that FLC4 cells do not support replication of these HCV RNAs (data not shown). Therefore, subsequent experiments were carried out with a stable Huh-7 cell line, RCYM1, which supports full-length HCV RNA replication and which was developed by transfection of the cells with genome-length dicistronic RNA derived from the Con1 clone I389neo/core-3′/NK 5.1 (genotype 1b)

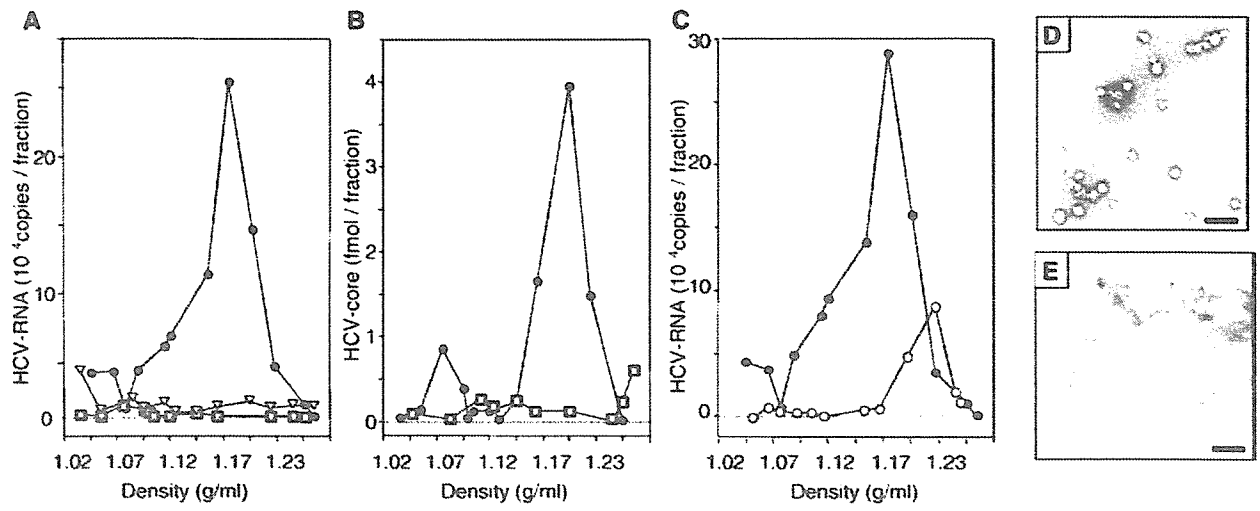

Fig. 1. Sucrose density gradient analysis of culture supernatants of RCYM1 cells. Culture media collected from radial-flow bioreactor (RFB)-cultured RCYM1 (closed circles), monolayer-cultured RCYM1 (open squares), and RFB-cultured 5–15 cells (open triangles) were fractionated as described in Materials and methods. (A) HCV RNA in each fraction was measured by real-time reverse transcriptase-polymerase chain reaction (RT-PCR). Mean values of duplicates were plotted against the density of the corresponding fraction. (B) HCV core protein in each fraction was determined by enzyme-linked immunosorbent assay (ELISA). Mean values of duplicates were plotted against the density. (C) Culture medium of RFB-cultured RCM1 cells were treated with 0.2% NP40 (open circles), followed by centrifugation in a sucrose gradient. Each fraction was tested for HCV RNA by real-time RT-PCR. (D, E) Electron microscopy analysis. Samples were prepared from the 1.18 g/ml fraction of culture media collected from RFB-cultured (D) or monolayer-cultured (E) RCYM1 cells.

(Pietschmann et al., 2002). The HCV RNA level in RCYM1 cells was approximately 5×10^6 copies/μg total RNA as determined by real-time reverse transcriptase-polymerase chain reaction (RT-PCR). The expression and subcellular localization of HCV protein were confirmed by Western blotting and immunofluorescence analysis (data not shown). To develop 3D RFB cultures, first we loaded RCYM1 cells onto an RFB column by flowing cell suspension, after which the cells were attached to carrier beads. Cells proliferated within the 3D matrix, and culture medium was circulated radially through the column.

In order to investigate whether HCV-like particles (HCV-LPs) were secreted from RCYM1 cells in the RFB culture system, we fractionated culture fluid collected after 5–10 days of culture by continuous 10–60% (wt/vol) sucrose density gradient centrifugation. HCV RNA and core protein were predominantly detected in the 1.15–1.20 g/ml fractions, with maximal detection in the 1.18 g/ml fraction (Figs. 1A and B). In the same experiment using 5–15 cells, in which a subgenomic HCV replicon replicates, no peak similar to that observed in RCYM1 cells corresponding to HCV RNA was detected. In both RCYM1 cells and 5–15 cells in the RFB culture system, a substantial amount of HCV RNA was detected in the 1.03–1.07 g/ml fractions (Fig. 1A). Consistent with a previous report by Pietschmann et al. (2002), these RNAs released from cells with a subgenomic replicon did not correspond to virus particles. When an equivalent number of RCYM1 cells were cultured in a monolayer culture system, limited amounts of HCV RNA and core protein were detected in the culture supernatant (Figs. 1A and B).

The mature HCV virion is thought to have a nucleocapsid and an outer envelope composed of a lipid membrane with viral envelope glycoproteins. Culture fluids were treated with NP40 in order to solubilize lipids and were then subjected to sucrose density gradient centrifugation. HCV RNA sedimented to a density of 1.22 g/ml rather than 1.18 g/ml (Fig. 1C), indicating that the density of HCV particles became higher due to de-envelopment. Transmission electron microscopy (TEM) of the 1.18 g/ml fraction, which was subjected to negative staining after concentration, revealed particle structures with diameters of 30–60 nm and a major particle size of 50 nm (Fig. 1D). No similar particle-like structures were observed in the same density fraction of the RCYM1 monolayer culture (Fig. 1E) or in the 1.23 g/ml fraction of the RCYM1-RFB culture (data not shown). These results indicate that, in the RFB system, the production and secretion of HCV-LPs is possible with a selectable dicistronic HCV genome.

Production and secretion of HCV-LPs from spheroid culture of RCYM1 cells using TGP

In the 3D RFB culture system for RCYM1 cells, extracellular secretion of HCV-LPs was observed. Based on this observation, we hypothesized that morphological changes occurring in 3D culture, such as polarity formation, promote advantageous in the assembly of viral proteins, particle formation, and extracellular secretion. To examine whether similar phenomena could be observed in other 3D culture systems, we investigated HCV-LP expression using a 3D culture system with TGP as a carrier.

TGP is a biocompatible polymer made from conjugates of polyethyleneglycol and poly-*N*-isopropylacrylamide, which is a thermoresponsive polymer composed of *N*-isopropylacrylamide and *n*-butylmethacrylate. The TGP solution possesses sol-gel transition properties; it is water soluble (sol phase) at temperatures below the transition temperature, and it is insoluble (gel phase) above it. It is possible to manipulate the transition temperatures through molecular engineering. The transition temperature for TGP in the present experiments was approximately 20 °C.

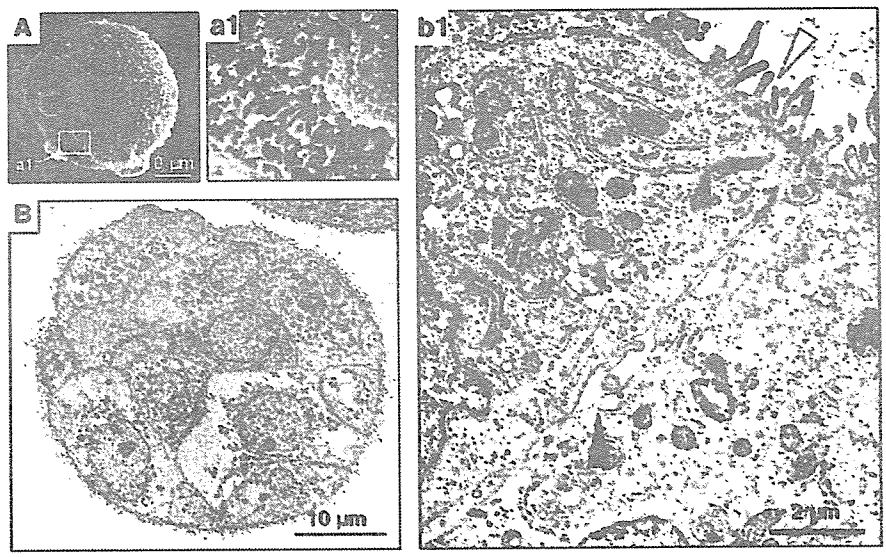

Fig. 2. Huh-7 and RCYM1 cells form spheroids in thermoreversible gelation polymer (TGP). Scanning electron microscopy (A and a1) and transmission electron microscopy (B and b1) of RCYM1 cells cultured in TGP for 8 days. Open arrowhead, microvilli; closed arrowheads, bile canaliculi-like structures.

RCYM1 cells, which were seeded into the TGP, formed three-dimensional compacted aggregates called spheroids after 3 days of culture, and numerous spheroids with diameters of approximately 1 mm were observed after 7–10 days of culture. After 8 days of culture, the spheroids were fixed and examined by scanning electron microscopy (Figs. 2A and a1) and ultrathin sections were examined by TEM (Figs. 2B and b1). Well-developed microvilli, a feature of polarized epithelium, were observed on the cell surface (Figs. 2A and a1). Bile canaliculi-like structures were also observed within intercellular spaces, and they appeared to be connected via tight junctions (Figs. 2B and b1). This cytomorphology, similar to that observed in the RFB culture (Kawada et al., 1998; Matsuura et al., 1998), correlated well with the features of mature liver tissue.

It is known that the replication of HCV replicons in Huh-7 cells depends on host cell growth. We found that the growth of RCYM1 cells in the TGP culture system was significantly slower than that of cells in monolayer culture (Fig. 3A). Accordingly, the expression of HCV proteins (Fig. 3B) in the RCYM1 spheroids was apparently lower compared to those observed in the monolayer cells. The viral RNA copy number in the spheroids was approximately one tenth of that in the monolayer culture (data not shown). The results of sucrose density gradient analysis of culture supernatant demonstrated co-sedimentation of HCV RNAs and core proteins at a density of 1.15–1.20 g/ml, with a peak at 1.18 g/ml (Figs. 3C and D). This distribution was consistent with the pattern obtained in RFB culture (Figs. 1A and B). It should be noted that in these experiments, lower cell numbers were used in the 3D cultures than in the monolayer cultures because of the slower growth of cells. As estimated from the quantitative data of the 1.15–1.20 g/ml fractions of the culture supernatants, 0.1–1 copies of HCV RNA/cell/day are produced and assembled into viral particles in the TGP-cultured RCYM1 cells.

TEM analysis of the 1.18 g/ml fraction after negative staining showed particle structures with a diameter of 50–60 nm and spike-like projections (Fig. 3E). Observation of ultrathin sections indicated a lipid bilayer-like membrane structure with a

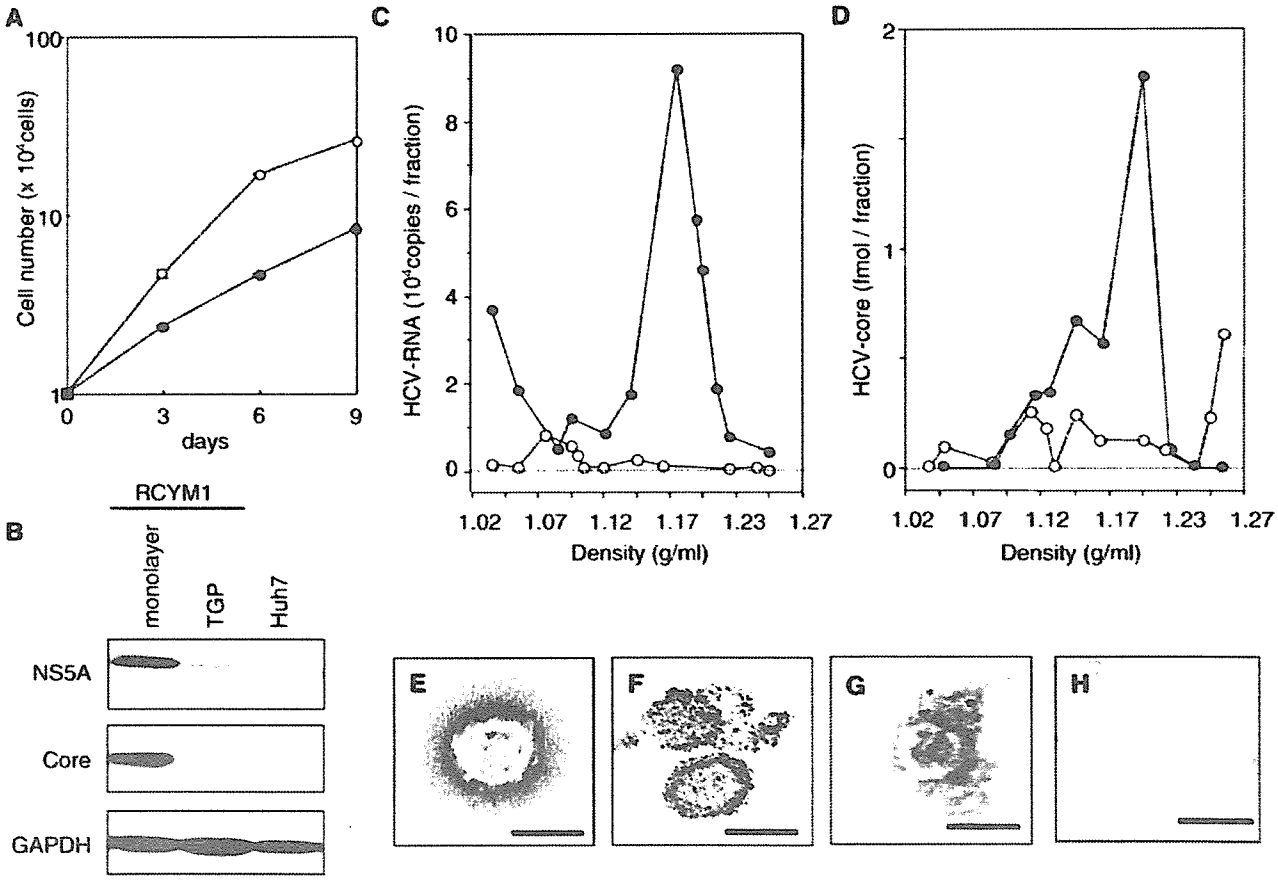

Fig. 3. Expression of HCV proteins in RCYM1 cells and secretion of viral particles in TGP culture. (A) Cell growth curves of the TGP (closed circles) and monolayer (open circles) culture of RCYM1 cells. Cells were harvested at days 0, 3, 6, and 9 postinoculation and cell numbers were determined. (B) Western blotting of HCV core and NS5A proteins in RCYM1 cells and control Huh-7 cells. (C, D) Sucrose density gradient analysis of culture supernatants of RCYM1 cells. The culture supernatants were fractionated as described in Materials and methods. HCV RNA (C) and core protein (D) in each fraction were determined by ELISA and real-time RT-PCR, respectively. Representative data from three independent experiments are shown. Closed circles, TGP culture; open circles, monolayer culture. (E–H) Electron microscopy of HCV-like particles (HCV-LPs) in the supernatants of TGP-cultured RCYM1 cells. (E) Negative staining of HCV-LPs in the 1.18 g/ml density fraction. There was no spherical structure in 1.05 g/ml density fraction, as shown in panel H. (F) Ultrathin section of HCV-LPs. Precipitated HCV-LP samples were prepared from the 1.18 g/ml fraction as described in Materials and methods. (G) Immunogold labeling of HCV-LPs with an anti-E2 antibody in the 1.18 g/ml density fraction. Gold particles, 5 nm; scale bars, 50 nm.

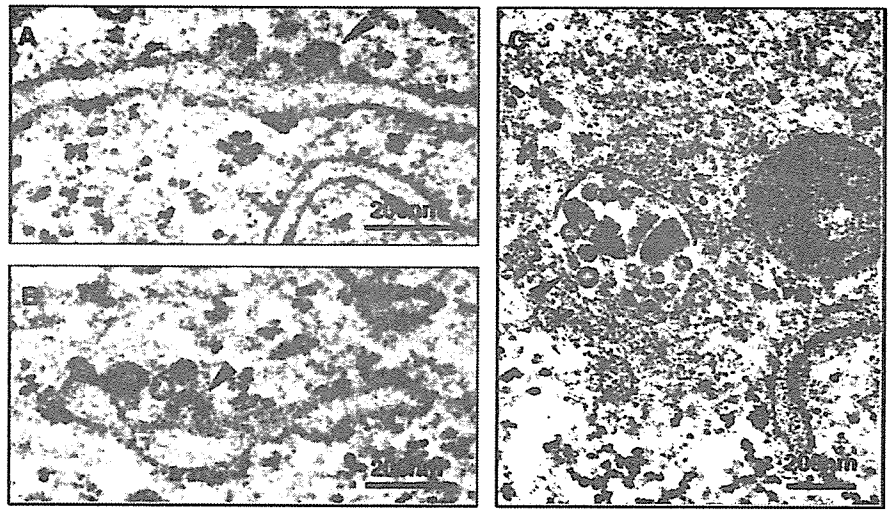

Fig. 4. Electron microscopy of ultrathin sections of RCYM1 cells grown in TGP. HCV-LPs in TGP-cultured RCYM1 cells. Spherical virus-like particles 50–60 nm in diameter (arrowheads) were observed at the ER membranes (A, B) and in the cytoplasmic vesicles (C).

width of approximately 5 nm (Fig. 3F). Immunoelectron microscopic study using anti-E2 antibody revealed HCV envelope protein(s) on the particle surface (Fig. 3G). Substantial amounts of HCV RNA were detected in the 1.03–1.05 g/ml fractions of the supernatant (Fig. 3C); however, HCV-LP structures were not observed in these fractions (Fig. 3H). These results were consistent with those from the RFB system, as shown above. The efficacy of 3D cell culture systems in virion formation was thus demonstrated in both the RFB and TGP culture systems using human liver-derived cells.

Ultrastructural localization of HCV-LPs in TGP-cultured spheroids of RCYM1 cells

We next determined the intracellular localization of HCV-LPs produced in RCYM1-TGP culture at the ultrastructural level by electron microscopic (EM) analysis of ultrathin sections. Spherical particles having membrane-like structures with short surface projections (diameter, 50–60 nm) were observed primarily at the endoplasmic reticulum (ER) membrane (Fig. 4A) as well as in the dilated cisternae of the ER (Fig. 4B). In vesicles, these virus-like particles were frequently associated with amorphous materials (Fig. 4C). In a previous study, **Shimizu et al. (1996)** report that virus-like particles with similar morphology and size were observed in human B cells infected with HCV. No similar particle-like structures were observed in RCYM1 cells in monolayer culture or in subgenomic replicon 5–15 in cells in TGP culture (data not shown).

In order to determine whether the virus-like particles observed by conventional TEM in the present experiment were HCV-LPs, we conducted immunoelectron microscopic analysis with anti-core antibody and anti-E1 antibody. Double-labeling experiments showed that the virus-like particles associated with the ER membrane exhibited immunoreactivity for both HCV proteins, and that the E1 protein surrounded the core proteins (Fig. 5A). To the best of our knowledge, this is the first report to clearly demonstrate that the viral envelope protein surrounds the core protein in HCV particle formation. As a negative control, thin sections prepared from subgenomic RNA containing 5–15 cells were stained with these antibodies and were found to exhibit negligible levels of background immunostaining (data not shown).

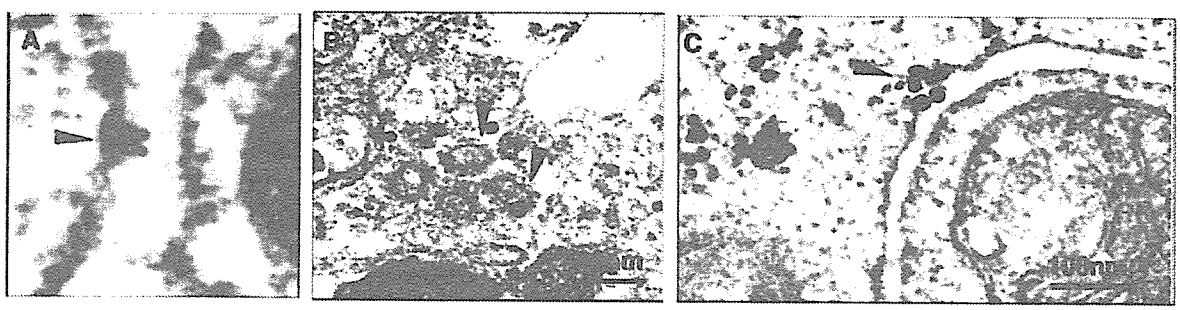

Fig. 5. Immunoelectron microscopy of ultrathin sections of TGP-cultured RCYM1 cells. (A) Double immunostaining with anti-E1 and anti-core monoclonal antibodies. Core protein-specific gold particles (10 nm in diameter) and E1 protein-specific gold particles (5 nm in diameter) formed rosettes on the surface of the ER membrane. (B and C) Silver-intensified immunogold staining with anti-core (B) and anti-E1 (C) antibodies. The second antibody conjugated with gold particles 1.4 nm in diameter was applied, followed by enlargement of the particles by the silver enhancement reagent. Arrowheads indicate virus-like particles reacting with anti-core and/or anti-E1 antibodies.

It is generally difficult to visualize intracellular microstructures and perform antigenic protein localizations using immunogold electron microscopy due to the low resolution and contrast of micrographs. In order to overcome this difficulty, we applied a silver-intensified immunogold labeling method in our experiment (Figs. 5B and C). Using this method, antigen-reactive immunogold particles approximately 20 nm in diameter were observed. Specific immunolabeling of core and E1 protein was detected in the ER or on the ER membranes. Intense immunopositive reactions were also seen on the virus-like particles observed in cytoplasmic vesicles and on ER membranes; however, no such immunolabeling was observed when normal mouse serum was used as a first antibody (data not shown). These results confirm the ultrastructural observations of conventional TEM and suggest that the formation of HCV particles is achieved by budding of the putative core particles at the ER membrane.

Infectivity of HCV-LPs depends on E2 glycoprotein

To determine whether HCV-LPs released from RCYM1 cells cultured in the TGP system are infectious, we inoculated naive Huh-7.5.1 cells (Zhong et al., 2005), which are HCV-negative Huh-7.5 (Blight et al., 2002)-derived cells, with a culture supernatant of RCYM1 spheroids. HCV RNAs in the cells at days 0, 1, 2, 3, and 7 postinoculation were determined by real-time RT-PCR. Fig. 6A shows the kinetics of HCV RNA after the inoculation of HCV-LPs. HCV RNA levels in the infected Huh-7.5.1 cells fluctuated at the indicated times, reaching 10^3–10^4 copies/μg of cellular RNA at days 1–7. Immunofluorescence staining 4 days postinoculation revealed that approximately 1% of cells were positive for NS5A protein (Fig. 6B). In contrast, no NS5A-positive cells were detected when the cell supernatant sample obtained from 5 to 15 cell cultured in TGP was used to inoculate Huh-7.5.1 cells (data not shown). These results suggest that HCV-LPs released from TGP-cultured RCYM1 cells are infectious.

To further determine whether viral envelope proteins mediate infection by HCV-LPs, we preincubated HCV-LPs with the anti-E2 monoclonal antibody AP33, which demonstrates potent neutralization of infectivity against HCV pseudoparticles carrying E1 and E2 proteins representative of the major genotypes 1 through 6 (Owsianka et al., 2005), or with patient sera with high titers of HCV neutralization of binding (NOB) antibodies (Ishii et al., 1998), or with anti-FLAG antibody (Fig. 6C). NOB antibodies have the ability to neutralize the binding of E2 protein to human cells (Rosa et al., 1996), and NOB3 and NOB4 were sera obtained from patients who recovered naturally from chronic hepatitis C (Ishii et al., 1998). Intracellular HCV RNA levels were decreased by 43%, 28%,

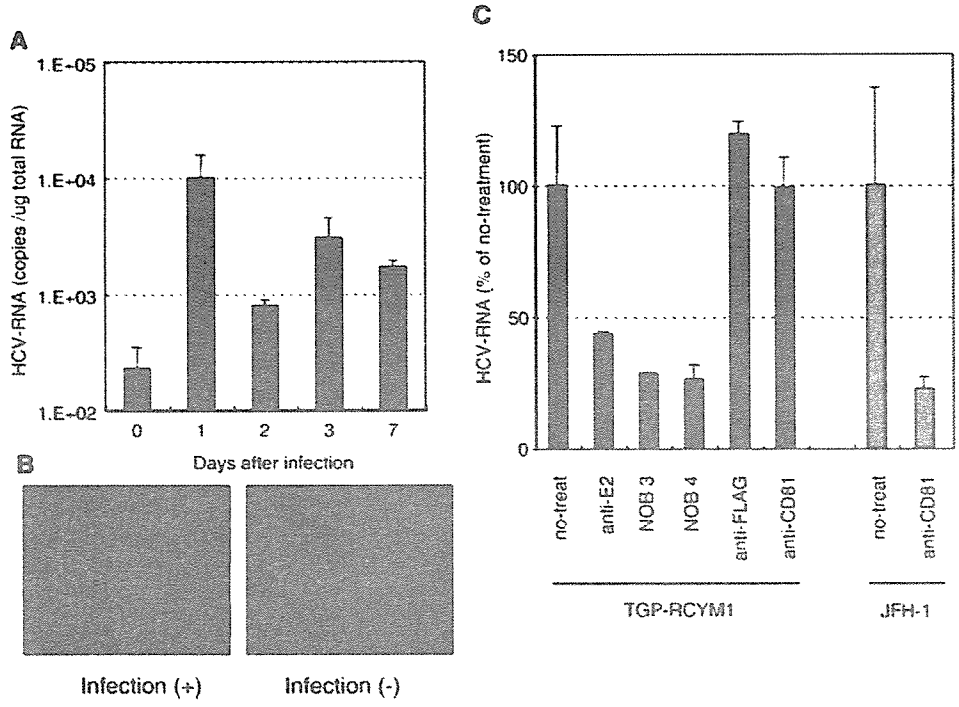

Fig. 6. Infectivity of HCV-LPs secreted from TGP-cultured RCYM1 cells and neutralization of the infection. (A) Kinetics of HCV RNA after the infection of HCV-LPs. Huh-7.5.1 cells were infected with HCV-LPs and harvested at days 0, 1, 2, 3, and 7. HCV RNAs in the cells were determined by real-time RT-PCR. (B) Huh-7.5.1 cells infected with HCV-LPs (upper panel) or without infection (lower panel) were cultured for 4 days, followed by immunostaining with anti-NS5A antibody. Nuclei were counterstained with 4′,6-diamidino-2-phenylindole (DAPI). (C) Huh-7.5.1 cells were infected with HCV-LPs after pretreatment with anti-E2 antibody AP33, neutralization of binding (NOB) antibodies, or anti-FLAG antibody. Anti-human CD81 antibody was preincubated with Huh-7.5.1 cells prior to the infection. Huh-7.5.1 cells were infected with HCV-LPs derived from TGP-cultured RCYM1 cells or JFH1 virus and incubated for 4 days; HCV RNAs in the cells were determined by real-time RT-PCR. The inhibition rate is given as the percentage of the no-treatment controls. Average values with standard deviations in triplicate samples are shown. Closed bars, HCV-LPs secreted from TGP-cultured RCYM1 cells; shaded bars, JFH1 virus.

and 26% in the presence of AP33, NOB3, and NOB4, respectively. No reduction of viral RNA in infected cells was observed following treatment with anti-FLAG antibody. Thus, the present results suggest that viral envelope proteins play a crucial role in the infectivity of HCV-LPs produced by RCYM1 cells cultured in TGP. We further tested anti-CD81 antibody for inhibition of the virus infection in our system. As shown in Fig. 6C, pretreatment of the cells with the anti-CD81 antibody resulted in no inhibition of the intracellular HCV RNA level in the infected cells. In contrast, under the same condition of treatment, the antibody efficiently inhibited the infection of JFH-1 virus, which was produced from the HCV JFH-1 molecular clone as previously described (Wakita et al., 2005; Zhong et al., 2005), suggesting that CD81 has no or little, if any, need for the infection of HCV produced in our system.

Potential use of the TGP culture system for HCV production and evaluation of antiviral agents

In a recent report, Lindenbach et al. (2005) found that a cell culture system supporting complete replication of an HCV genotype 2a clone is useful for the evaluation of antiviral drugs. However, to date this complete HCV culture system has not been extended to genotype 1b, which is more frequently detected in patients with hepatitis C and is the most difficult to treat.

We show here the potential utility of the TGP culture of RCYM1 cells for evaluating anti-HCV drugs (Fig. 7). Intracellular HCV RNA levels in TGP-cultured RCYM1 cell spheroids were reduced by 90% after 3 days of culture with 100 IU/ml of IFN-α (Fig. 7A). Likewise, the extracellular HCV particle level, which was calculated using the HCV RNA copy number of the 1.18 g/ml supernatant fraction, was reduced by 89% by IFN-α treatment (Fig. 7B). Moreover, the production of HCV particles was inhibited by treatment with 100 μM RBV to the same degree (85%) as intracellular HCV RNA (Fig. 7B). The level of HCV RNA detected in the 1.04 g/ml fraction of the culture supernatant of the untreated group was approximately one fourteenth of that in the 1.18 g/ml fraction, and the level increased with the addition of IFN-α or RBV (Fig. 7B). Although the mechanism underlying this increase is unknown, a similar phenomenon was observed when several highly cytotoxic agents were evaluated using TGP-RCYM1 cultures (data not shown). It is therefore likely that some cellular proteins associated with HCV RNA are released into the culture supernatant as a result of cell death caused by the moderate cytotoxic effects of IFN and RBV.

Collectively, these results demonstrate that the HCV production model based on TGP culture is useful for evaluating HCV particle production and the inhibitory effects of anti-HCV drugs.

Discussion

In the present report, we describe that HCV-LPs are assembled and released from Huh-7 cells harboring a dicistronic genome-length Con1 HCV RNA in two independent 3D culture systems. The HCV-LPs closely resemble virus-like particles detected in the sera of patients with hepatitis C in terms of both particle size and morphology. The HCV-LPs released into the culture supernatant have a buoyant density of approximately 1.18 g/ml, which is much higher than that of putative HCV particles isolated from patient sera reported previously (Andre et al., 2002; Kanto et al., 1994; Nakajima et al., 1996; Trestard et al., 1998) and slightly higher than the average density of virus particles produced with the JFH-1 isolate (Wakita et al., 2005). One possible explanation is that the HCV particles are highly bound to lipids and low-density lipoproteins in patient sera. In agreement with a recent report (Wakita et al., 2005), our EM examination demonstrated that HCV-LPs are 50–60 nm in diameter and are composed of core-like particles with a diameter of approximately 30 nm that are surrounded by ER-derived E1/

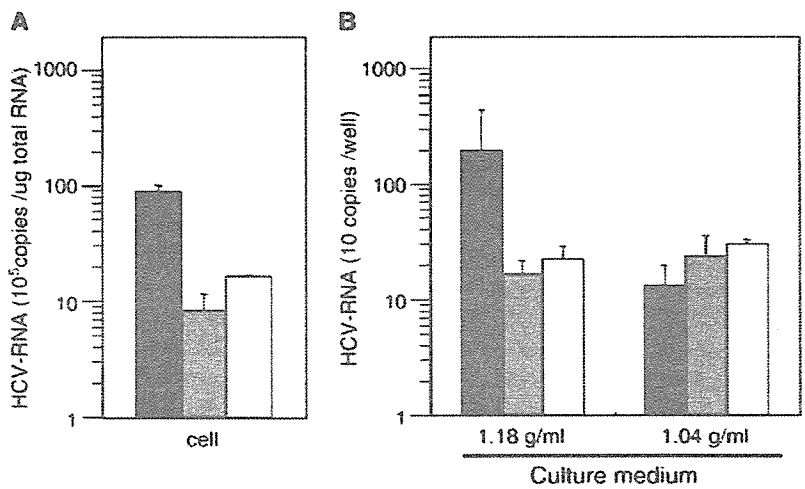

Fig. 7. Inhibition of HCV-LP production by IFN and RBV. TGP-cultured RCYM1 cells were treated with 100 IU/ml IFN-α or 100 μM RBV, and HCV RNAs in the cells (A) and in the culture media (B) were then determined. Culture media from each sample were fractionated by sucrose gradient centrifugation and HCV-LP positive (1.18 g/ml) and negative (1.04 g/ml) fractions were assayed. Average values with standard deviations in triplicate samples are shown. Closed bars, no-treatment control; shaded bars, IFN-α; open bars, RBV.

E2 proteins. These particles are observed at the ER membranes and in dilated cisternae of the ER, suggesting that the interaction of the ER membrane containing HCV envelope proteins with the viral core protein drives the budding process of HCV particles into the ER lumen.

Although studies on the ultrastructure and morphogenesis of HCV-LPs have been conducted using recombinant viral vectors carrying HCV structural protein genes (**Baumert et al., 1998**; **Blanchard et al., 2002, 2003**), the present study provides the first visual evidence of assembly and budding of HCV particles in a heterologous expression system in which a full-length viral genome is replicating and the viral particles are secreted into the culture medium. We also demonstrated that the HCV-LPs produced in our 3D culture system are infectious and that their infection is prevented by the monoclonal antibody AP33 directed against E2 (**Owsianka et al., 2005**) as well as by NOB antibodies (**Ishii et al., 1998**), which are sera of patients naturally resolving from chronic hepatitis C and exhibiting neutralizing activity. This result is consistent with the recent demonstration that E2 is required for the infectivity of JFH-1 virus (**Wakita et al., 2005**). It has been shown that CD81 interacts with E2 (**Pileri et al., 1998**) and that anti-CD81 antibodies or a soluble CD81 fragment block the infection of Huh-7 cells with either pseudotyped retroviral particles, JFH-1 virus or J6/JFH1 chimera (**Lindenbach et al., 2005**; **Netski et al., 2005**; **Wakita et al., 2005**; **Zhong et al., 2005**). Inconsistent with these studies, however, we found that anti-CD81 antibody did not inhibit the virus infection in our system. Although CD81 is considered to represent an important component in HCV entry, there are several other candidate cellular receptors for HCV (**Bartosch and Cosset, 2006**) and a study has demonstrated that in vitro binding of HCV to hepatoma cell lines was not inhibited by the anti-CD81 antibody (**Sasaki et al., 2003**).

In a previous report (**Aizaki et al., 2003**), we describe the production and release of infectious HCV particles from a human hepatocellular carcinoma-derived cell line, FLC4, using RFB culture in two experiments: inoculation of cells with infectious plasma from an HCV carrier and transfection of cells with viral RNA transcribed from the full-length cDNA of genotype 1a, which is known to infect chimpanzees. These findings prompted us to use the RFB system to create a culture model of HCV production based on genome-length dicistronic viral RNA, which has not been found to produce viral particles in standard monolayer cultures. As expected, HCV-LPs were produced and secreted into the medium during RFB culture of RCYM1 cells, whereas virus production was not observed in the conventional monolayer culture of RCYM1 cells. The presence of the viral envelope protein(s) on the HCV-LPs obtained in the RFB culture was strongly suggested from their density analysis with and without NP40 treatment.

We also created another 3D environment supportive of RCYM1 culture using TGP, a chemically synthesized biocompatible polymer which has a sol-gel transition temperature, thus enabling us to culture cells three-dimensionally in the gel phase at 37 °C and to harvest them in the sol phase at 4 °C, without enzyme digestion (**Yoshioka et al., 1994**). In contrast to other matrix gels made from conventional natural polymers and developed for 3D culture, including matrigel (**Kleinman et al., 1986**), collagen gel (**Lawler et al., 1983**), and soft agar, TGP has several advantages that allow us to investigate the functional characteristics of epithelial cells, their tissue-like morphology, and their potential clinical applications. The use of 3D culture materials other than TGP requires treatment with appropriate digestive enzymes or heating to collect cells grown as spheroids from the culture media, and the matrices may damage the cultured cells to some extent. Thus, it is difficult to keep the viable cells in a functionally and structurally intact. In addition, because matrigel and collagen gel are made from animal or tumor tissue, the possibility that certain pathogens or unidentified factors might influence cell function cannot be excluded. In the present study, we found that Huh-7 and RCYM1 cells formed an organized structure of spheroids after 7–10 days of culture in TGP, and that HCV-LPs were assembled and released from RCYM1 spheroids, as observed in RFB culture. It can be ruled out that HCV-LPs, RNA, and core protein detected in the TGP culture supernatant are released by damaged and/or broken cells because neither digestive enzymes nor heating is used in the culture procedures and no cell damage has been observed in the cultures.

It remains to be clarified why HCV particles were produced from Huh-7 cells harboring the genome-length dicistronic HCV RNA more efficiently in the 3D cultures than in the monolayer cultures. However, this might be related to the fact that directional protein transport in hepatocytes occurs more readily in 3D culture. EM examination demonstrated that, in the RFB and TGP culture systems, human hepatoma cells, such as Huh-7, FLC4, and FLC5 cells, self-assemble into spheroids with possible polarized morphology in which microvilli develop on the cell surface and channels resembling bile canaliculi and junction structures are created in the intercellular spaces (**Aizaki et al., 2003**; **Iwahori et al., 2003**). In contrast, human hepatoma cells adhere when grown on a plastic surface, growing as a flat monolayer without exhibiting the characteristics of polarized epithelium. In general, the interaction of viruses with polarized epithelia in the host is one of the key steps in the viral life cycle. A variety of viruses, especially enveloped viruses, mature and bud from distinct membrane domains of the host cells (**Compans, 1995**; **Garoff et al., 1998**; **Schmitt and Lamb, 2004**; **Takimoto and Portner, 2004**). For example, several respiratory viruses, such as influenza virus, parainfluenza virus, rhinovirus, and respiratory syncytial virus, are released preferentially from the apical surface. Conversely, other viruses egress from the basolateral membrane; these include vesicular stomatitis virus, Semliki Forest virus, vaccinia virus, and certain retroviruses. Thus, it is likely that more organized intracellular trafficking pathways exist in the 3D culture of Huh-7-derived cells, thereby driving the assembly and release of HCV.

The efficient production of HCV in 3D cultures could also be due to the reduction of HCV RNA replication and/or translation in 3D cultures as compared to those in monolayer cultures. RNA replication and/or translation of HCV replicons in Huh-7 cells are highly dependent on host cell growth (**Pietschmann et al., 2001**). In the present study, we found that the slow growth of spheroids resulted in reduced expression of HCV protein and

viral RNA in 3D-cultured RCYM1 cells compared to that in monolayer cultures containing similar cell numbers. The doubling time of cells grown in TGP or RFB culture was approximately twice that observed in monolayer culture. Although it is possible that amino acid substitutions of culture-adaptive mutations contribute to interference with virus production, another possibility might be that in cases of certain HCV clones, higher expression of the viral proteins leads to their misfolding, thereby precluding the formation of virus particles.

Complete cell culture systems for HCV have recently been developed (**Lindenbach et al., 2005**; **Wakita et al., 2005**; **Zhong et al., 2005**) using a genotype 2a isolate, JFH-1, obtained from a Japanese patient with fulminant hepatitis (**Date et al., 2004**; **Kato et al., 2001, 2003**). Unlike many other HCV isolates, JFH-1-based subgenomic replicons do not require culture-adaptive mutations for efficient RNA replication (**Kato et al., 2003**). Transfection of Huh-7 cells with the full-length JFH-1 genome or a chimeric genome using JFH-1 and J6 results in the efficient production of infectious HCV (**Lindenbach et al., 2005**; **Wakita et al., 2005**; **Zhong et al., 2005**). This newly established HCV culture system is undoubtedly useful for a variety of HCV studies; however, these systems rely on the JFH-1 replicase (NS3 to 5B) and little is known about the reasons that this particular isolate permits efficient HCV production. Virus yield in the 3D systems presented here is significantly lower than that in systems based on JFH-1; it seems that 0.1–1 copies of HCV RNA/cell/day are generated and assembled into viral particles. The ratio of viral RNA to the core protein in these fractions is approximately 10^5 RNA copies/1 fmol of the core. Although only moderate production of HCV particles is observed in 3D culture of RCYM1 cells, this is the first study to demonstrate the production of infectious HCV particles derived from genotype 1b, which is highly prevalent worldwide and is thought to present a higher risk of developing hepatocellular carcinoma and/or cirrhosis than infections with other HCV types (**Bruno et al., 1997**; **Silini et al., 1996**). The findings of the present study may also suggest that an extremely high efficiency of viral replication, such as that observed in the case of JFH-1 isolate, is not needed to produce HCV particles in 3D cultures of Huh-7 cells. **Heller et al. (2005)** report HCV virion production in a culture transfected with the genomic cDNA of genotype 1b; however, the infectivity of the virus particles remains to be determined. More recently, it was shown that chimeric HCV containing structural proteins of genotypes 1a, 1b, or 3a was produced from fusion of the core to the p7 or NS2 region with downstream nonstructural regions of JFH1 clone, but that intergenotypic chimeras frequently yielded lower titers of infectious HCV compared to JFH1 or J6/JFH1 chimera (Pietschmann et al., personal communication). The 3D culture system described in the present study might be a helpful method of increasing the efficiency of assembly and release of intergenotypic chimeric HCV.

In summary, we found that the expression of dicistronic genome-length Con1 HCV RNA of genotype 1b in 3D-cultured Huh-7 cells yields infectious virus particles, and we demonstrated the usefulness for producing HCV particles of two 3D culture systems based on RFB and TGP, in which human hepatoma cells can assemble into spheroids with potentially polarized morphology. HCV morphogenesis occurs in a complex cellular environment in which host factors may either enhance or reduce the assembly and budding process. The culture system described here will allow us to further study viral morphogenesis and the biophysical properties of HCV particles, and it provides a new tool for the future development of anti-HCV drugs.

Materials and methods

Cell lines bearing dicistronic HCV RNAs

To generate a stable cell line harboring genome-length dicistronic HCV RNA, we electroporated 10^7 Huh-7 cells with 50 μg of the RNA transcribed from a plasmid pFKI389neo/core-3′/NK5.1 (**Pietschmann et al., 2002**). The cells were maintained in Dulbecco's modified Eagle's medium with 10% fetal bovine serum and 0.5 mg/ml G418 (Promega). After stringent selection for 3 weeks, a fast-growing clone was isolated and designated as RCYM1. A Huh-7-derived cell line, 5–15, harboring a subgenomic replicon (**Lohmann et al., 1999**) was also used.

3D cell cultures

The RFB system (Able, Japan) was manipulated as described previously (**Aizaki et al., 2003**) with minor modifications. Briefly, the RFB column, being filled with 4 ml of porous carrier beads made from polyvinyl alcohol, seeded with 1×10^7 of RCYM1 or 5–15 cells. The cells were cultured in ASF104 medium (Ajinomoto, Japan) supplemented with 4 g/l of D-glucose, 2% fetal calf serum, and 0.5 mg/ml of G418 (Promega). TGP (Mebiol Gel MB-10; Mebiol, Japan) was supplied as a lyophilized form and its aqueous solution was prepared before use as previously described (**Hishikawa et al., 2004**; **Nagaya et al., 2004**; **Yoshioka et al., 1994**). Briefly, TGP in a flask was dissolved in 10 ml of the culture medium and was maintained at 4 °C overnight. To prepare HCV particles, we suspended 5×10^6 cells of RCYM1 in 10 ml of TGP solution and aliquots were poured into a multi-well plate. Upon warming to 37 °C, the TGP solution quickly turned into a gel form, and 3 volumes of the culture medium were added to cover the gel. To recover spheroid cells and the culture supernatant after cultivation, we subjected the cultured plate to a temperature of 4 °C for 10 min to dissolve the gel. In order to separate spheroid cells from the culture medium, we subsequently centrifuged the TGP culture diluted with the overlaid culture medium at 1000×*g* for 5 min.

Sucrose density gradient centrifugation

The culture medium collected from the RFB or TGP was centrifuged at 8000 × *g* for 50 min to remove all cellular debris, after which the supernatant was centrifuged at 25,000 rpm at 4 °C for 4 h with an SW28 rotor (Beckman). The precipitant was suspended in 1 ml of TNE buffer [10 mM Tris–HCl (pH 7.8), 1 mM EDTA, 100 mM NaCl] and was then layered on top of continuous 10–60% (wt/vol) sucrose gradient in TNE buffer,

followed by centrifugation at 35,000 rpm at 4 °C for 14 h with an SW41E rotor (Beckman). Fractions (1 ml each) were collected from the top of the tube (12 fractions in total). The density of each fraction was determined by the weight of 100 μl of the fraction. For NP40 treatment, 0.5 ml of the TNE-suspended sample as described above was supplemented with 10 μl of RNase inhibitor (Takara, Japan) and 5 μl of 1M DTT, which was diluted by adding NP40 solution to a final concentration of 0.2%. After incubation at 4 °C for 20 min, the sample was fractionated by discontinuous 10–60% sucrose gradient centrifugation.

Quantitation of HCV RNA and core protein

Total RNA was extracted from cells and from the culture medium using TRIZOL (Invitrogen) and a QIAamp Viral RNA Mini spin column (Qiagen), respectively. Real-time RT-PCR was performed using TaqMan EZ RT-PCR Core Reagents (PE Applied Biosystems), as described previously (Aizaki et al., 2004; Suzuki et al., 2005). HCV core antigen within cells and culture medium was measured by immunoassay (Ortho HCV-Core ELISA Kit; Ortho-Clinical Diagnotics), following the manufacturer's instructions.

Western blot analysis

The protein concentration of cells recovered from monolayer or 3D cultures was determined by BCA Protein Assay Kit (Pierce). Aliquots of samples were analyzed by sodium dodecyl sulfate–polyacrylamide gel electrophoresis (SDS–PAGE) and transferred to polyvinylidene difluoride membranes (Immobilon; Millipore, Japan) using a semidry blotter. After overnight incubation at 4 °C in blocking buffer (Dainippon Pharmaceuticals, Japan) with 0.2% Tween 20, the membranes were incubated with appropriately diluted anti-HCV core (Anogen) and anti-NS5A (Austral Biologicals) monoclonal antibody, followed by incubation with horseradish peroxidase conjugated anti-mouse immunoglobulin G (Cell Signaling). The blots were then washed and developed with enhanced SuperSignal West Pico Chemiluminecent Substrate (Pierce).

Immunocytochemistry

For NS5A staining, infected cells cultured on collagen-coated coverslips were washed with phosphate buffered saline (PBS) and fixed with 4% paraformaldehyde at 4 °C for 30 min, followed by permeabilization with PBS containing 0.2% TritonX-100. After preincubation with BlockAce (Dainippon Pharmaceuticals), the samples were stained using mouse anti-NS5A antibody and rhodamine-conjugated goat anti-mouse IgG (ICN Pharmaceuticals) as the first and second antibodies, respectively.

Electron microscopy

To visualize HCV-LPs secreted into the medium, we concentrated and adsorbed sucrose density fractions prepared as described above onto carbon-coated grids for 1 min. The grids were stained with 1% uranyl acetate for 1 min and examined under a Hitachi H-7600 transmission electron microscope. To prepare thin sections of HCV-LPs, we prefixed precipitated HCV-LPs in 2% glutaraldehyde–0.1 M cacodylate buffer at 4 °C overnight, followed by three rounds of washing with 0.1 M cacodylate buffer. The samples were then postfixed in 2% osmium tetroxide at 4 °C for 2 h, dehydrated in a graded series of ethanol solutions followed by propylene oxide, and embedded in a mixture of EPON 812, dodecenyl succinic anhydride (DDSA), methyl nadic anhydrate (MNA), and 2,4,6-tri (dimethylaminomethyl) phenol (DMP-30) at 60 °C for 2 days. Thin sections (80 nm) were stained with uranyl acetate and lead citrate. For electron microscopy of RCYM1 cells cultured in TGP, the cells were prefixed in 2% glutaraldehyde–0.1 M cacodylate buffer at 4 °C for 1 h and washed three times with 0.1 M cacodylate buffer, followed by postfixation in 2% osmium tetroxide for 3 h. After dehydration in a graded series of ethanol solutions and propylene oxide, the cells were embedded in a mixture of Epoxy 812, DDSA, MNA, and DMP-30 at 60 °C for 2 days. Thin sections (60–80 nm) were stained with 2% uranyl acetate.

Immunoelectron microscopy

HCV-LP samples were adsorbed on formvar-carbon grids and then floated for 30 min on a drop of BlockAce. Diluted anti-E2 mouse antibody was then applied for 1 h. After three rounds of washing, diluted anti-mouse IgG conjugated with 5-nm gold particles was applied for 1 h, and the grids were then stained with 1% uranyl acetate. In order to perform immunoelectron microscopy of TGP cultures using silver-intensified immunogold labeling, we fixed the cells in 4% paraformaldehyde–0.1% glutaraldehyde with 0.15 M HEPES buffer at 4 °C, followed by incubation with either anti-core rabbit antibody or anti-E1 mouse antibody overnight. After several washings, anti-rabbit or anti-mouse secondary antibody coupled with 1.4-nm-diameter gold particles (Nanoprobes) was applied overnight. The samples were then washed and fixed in 2% glutaraldehyde in 0.1 M sodium cacodylate buffer (pH 7.4) for 3 h, followed by enlargement of the gold particles with an HQ-Silver Enhancement Kit (Nanoprobes). For double staining with anti-E1 and anti-core antibodies, the cells were fixed in 7% paraformaldehyde–0.25 M sucrose in 0.03% picric acid–0.05 M cacodylate buffer at pH 7.4. Ten-nanometer gold particle-coupled anti-rabbit and 5-nm gold particle-coupled anti-mouse antibodies were used as secondary antibodies.

Assays for the infectivity of HCV-LPs and neutralization of the infection

Cell supernatant from 3D-cultured RCYM1 cells was centrifuged at 8000 × *g* for 50 min to remove all cellular debris, after which the supernatant was centrifuged at 25,000 rpm at 4 °C for 4 h with an SW28 rotor. The precipitant was suspended in 0.2–0.5 ml of ASF104 medium and the aliquot containing approximately 1×10^5 HCV RNA copies was used as each inoculum. Huh-7.5.1

cells (provided by Dr. F. V. Chisari, The Scripps Research Institute) (Zhong et al., 2005), which were seeded at a density of 10^4 cells/well in a 48-well plate 24 h before infection. The inocula were incubated for 3 h, followed by 3 rounds of washing with PBS and the addition of complete medium. For the kinetics assay, cells were harvested 0, 1, 2, 3, and 7 days after infection and the amount of intracellular HCV RNA was quantified as described above. Infection with HCV-LP was determined after 4 days by immunofluorescence staining for HCV NS5A. In the neutralization assay, the HCV-LP samples were incubated with the anti-E2 antibody AP33 (Owsianka et al., 2005) at 10 μg/ml (kindly provided by Dr. A. H. Patel, University of Glasgow, UK), with the human sera with high titers of NOB antibodies NOB3 and NOB4 (Ishii et al., 1998), or with anti-FLAG antibody (Sigma) at 10 μg/ml for 1 h at 37 °C prior to infection. Anti-human CD81 antibody (BD Pharmigen) at 10 μg/ml was preincubated with Huh-7.5.1 cells for 1 h at 37 °C, followed by being washed with PBS three times. HCV-LP derived from TGP-cultured RCYM1 cells or JFH1 virus was incubated with these cells, as mentioned above. JFH1 virus was prepared from pJFH1 (Wakita et al., 2005), which contains the full-length cDNA of JFH1 isolate and was kindly provided by T. Wakita (Tokyo Metropolitan Institute for Neuroscience, Japan), as described (Wakita et al., 2005). The cells were harvested 4 days after infection and neutralizing activity was assessed by quantifying the amount of intracellular HCV RNA as described above.

Assay for anti-HCV-LP production

At the initiation of the 3D culture of RCYM1 cells (5×10^5 in 1 ml TGP), 100 IU/ml IFN-α (Sumiferon 300; Sumitomo Pharmaceuticals, Japan), or 100 μM RBV (MP Biomedicals, Germany) were added and the cells were cultured for 5 days. Culture media were harvested and fractionated by sucrose density centrifugation as described above. Total RNAs were extracted from aliquots of 1.18 g/ml (HCV-LP positive) and 1.04 g/ml (HCV-LP-negative) fractions, followed by quantification of viral RNA.

Acknowledgments

The authors would like to thank Francis V. Chisari of The Scripps Research Institute, Arvind H. Patel of the University of Glasgow, and Takaji Wakita of Tokyo Metropolitan Institute for Neuroscience for providing Huh-7.5.1 cells, anti-E2 antibody, and pJFH1, respectively. We also thank Mami Matsuda, Tetsu Shimoji, and Makiko Yahata for technical assistance, and Tomoko Mizoguchi for her secretarial work. This work was supported in part by a grant for Research on Health Sciences focusing on Drug Innovation from the Japan Health Sciences Foundation; by grants-in-aid from the Ministry of Health, Labor and Welfare; by a Sasagawa Scientific Research Grant from the Japan Science Society; and by the program for Promotion of Fundamental Studies in Health Sciences of the National Institute of Biomedical Innovation (NBIO), Japan; and by the New Energy and Industrial Technology Development Organization (NEDO) of Japan.

References

Aizaki, H., Nagamori, S., Matsuda, M., Kawakami, H., Hashimoto, O., Ishiko, H., Kawada, M., Matsuura, T., Hasumura, S., Matsuura, Y., Suzuki, T., Miyamura, T., 2003. Production and release of infectious hepatitis C virus from human liver cell cultures in the three-dimensional radial-flow bioreactor. Virology 314, 16–25.

Aizaki, H., Lee, K.J., Sung, V.M., Ishiko, H., Lai, M.M., 2004. Characterization of the hepatitis C virus RNA replication complex associated with lipid rafts. Virology 324, 450–461.

Andre, P., Komurian-Pradel, F., Deforges, S., Perret, M., Berland, J.L., Sodoyer, M., Pol, S., Brechot, C., Paranhos-Baccala, G., Lotteau, V., 2002. Characterization of low- and very-low-density hepatitis C virus RNA-containing particles. J. Virol. 76, 6919–6928.

Bartosch, B., Cosset, F.L., 2006. Cell entry of hepatitis C virus. Virology (Electronic publication ahead of print).

Baumert, T.F., Ito, S., Wong, D.T., Liang, T.J., 1998. Hepatitis C virus structural proteins assemble into viruslike particles in insect cells. J. Virol. 72, 3827–3836.

Blanchard, E., Brand, D., Trassard, S., Goudeau, A., Roingeard, P., 2002. Hepatitis C virus-like particle morphogenesis. J. Virol. 76, 4073–4079.

Blanchard, E., Hourioux, C., Brand, D., Ait-Goughoulte, M., Moreau, A., Trassard, S., Sizaret, P.Y., Dubois, F., Roingeard, P., 2003. Hepatitis C virus-like particle budding: role of the core protein and importance of its Asp111. J. Virol. 77, 10131–10138.

Blight, K.J., Kolykhalov, A.A., Rice, C.M., 2000. Efficient initiation of HCV RNA replication in cell culture. Science 290, 1972–1974.

Blight, K.J., McKeating, J.A., Rice, C.M., 2002. Highly permissive cell lines for subgenomic and genomic hepatitis C virus RNA replication. J. Virol. 76, 13001–13014.

Bruno, S., Silini, E., Crosignani, A., Borzio, F., Leandro, G., Bono, F., Asti, M., Rossi, S., Larghi, A., Cerino, A., Podda, M., Mondelli, M.U., 1997. Hepatitis C virus genotypes and risk of hepatocellular carcinoma in cirrhosis: a prospective study. Hepatology 25, 754–758.

Choo, Q.L., Kuo, G., Weiner, A.J., Overby, L.R., Bradley, D.W., Houghton, M., 1989. Isolation of a cDNA clone derived from a blood-borne non-A, non-B viral hepatitis genome. Science 244, 359–362.

Choo, Q.L., Richman, K.H., Han, J.H., Berger, K., Lee, C., Dong, C., Gallegos, C., Coit, D., Medina-Selby, R., Barr, P.J., et al., 1991. Genetic organization and diversity of the hepatitis C virus. Proc. Natl. Acad. Sci. U.S.A. 88, 2451–2455.

Compans, R.W., 1995. Virus entry and release in polarized epithelial cells. Curr. Top. Microbiol. Immunol. 202, 209–219.

Date, T., Kato, T., Miyamoto, M., Zhao, Z., Yasui, K., Mizokami, M., Wakita, T., 2004. Genotype 2a hepatitis C virus subgenomic replicon can replicate in HepG2 and IMY-N9 cells. J. Biol. Chem. 279, 22371–22376.

Davis, G.L., Wong, J.B., McHutchison, J.G., Manns, M.P., Harvey, J., Albrecht, J., 2003. Early virologic response to treatment with peginterferon alfa-2b plus ribavirin in patients with chronic hepatitis C. Hepatology 38, 645–652.

Frese, M., Pietschmann, T., Moradpour, D., Haller, O., Bartenschlager, R., 2001. Interferon-alpha inhibits hepatitis C virus subgenomic RNA replication by an MxA-independent pathway. J. Gen. Virol. 82, 723–733.

Garoff, H., Hewson, R., Opstelten, D.J., 1998. Virus maturation by budding. Microbiol. Mol. Biol. Rev. 62, 1171–1190.

Grakoui, A., McCourt, D.W., Wychowski, C., Feinstone, S.M., Rice, C.M., 1993. Characterization of the hepatitis C virus-encoded serine proteinase: determination of proteinase-dependent polyprotein cleavage sites. J. Virol. 67, 2832–2843.

Guo, J.T., Bichko, V.V., Seeger, C., 2001. Effect of alpha interferon on the hepatitis C virus replicon. J. Virol. 75, 8516–8523.

Heller, T., Saito, S., Auerbach, J., Williams, T., Moreen, T.R., Jazwinski, A., Cruz, B., Jeurkar, N., Sapp, R., Luo, G., Liang, T.J., 2005. An in vitro model of hepatitis C virion production. Proc. Natl. Acad. Sci. U.S.A. 102, 2579–2583.

Hijikata, M., Kato, N., Ootsuyama, Y., Nakagawa, M., Shimotohno, K., 1991. Gene mapping of the putative structural region of the hepatitis C virus genome by in vitro processing analysis. Proc. Natl. Acad. Sci. U.S.A. 88, 5547–5551.

Hishikawa, K., Miura, S., Marumo, T., Yoshioka, H., Mori, Y., Takato, T., Fujita, T., 2004. Gene expression profile of human mesenchymal stem cells during osteogenesis in three-dimensional thermoreversible gelation polymer. Biochem. Biophys. Res. Commun. 317, 1103–1107.

Ikeda, M., Yi, M., Li, K., Lemon, S.M., 2002. Selectable subgenomic and genome-length dicistronic RNAs derived from an infectious molecular clone of the HCV-N strain of hepatitis C virus replicate efficiently in cultured Huh7 cells. J. Virol. 76, 2997–3006.

Ishii, K., Rosa, D., Watanabe, Y., Katayama, T., Harada, H., Wyatt, C., Kiyosawa, K., Aizaki, H., Matsuura, Y., Houghton, M., Abrignani, S., Miyamura, T., 1998. High titers of antibodies inhibiting the binding of envelope to human cells correlate with natural resolution of chronic hepatitis C. Hepatology 28, 1117–1120.

Iwahori, T., Matsuura, T., Machashi, H., Sugo, K., Saito, M., Hosokawa, M., Chiba, K., Masaki, T., Aizaki, H., Ohkawa, K., Suzuki, T., 2003. CYP3A4 inducible model for in vitro analysis of human drug metabolism using a bioartificial liver. Hepatology 37, 665–673.

Kanto, T., Hayashi, N., Takehara, T., Hagiwara, H., Mita, E., Naito, M., Kasahara, A., Fusamoto, H., Kamada, T., 1994. Buoyant density of hepatitis C virus recovered from infected hosts: two different features in sucrose equilibrium density-gradient centrifugation related to degree of liver inflammation. Hepatology 19, 296–302.

Kato, T., Furusaka, A., Miyamoto, M., Date, T., Yasui, K., Hiramoto, J., Nagayama, K., Tanaka, T., Wakita, T., 2001. Sequence analysis of hepatitis C virus isolated from a fulminant hepatitis patient. J. Med. Virol. 64, 334–339.

Kato, T., Date, T., Miyamoto, M., Furusaka, A., Tokushige, K., Mizokami, M., Wakita, T., 2003. Efficient replication of the genotype 2a hepatitis C virus subgenomic replicon. Gastroenterology 125, 1808–1817.

Kawada, M., Nagamori, S., Aizaki, H., Fukaya, K., Niiya, M., Matsuura, T., Sujino, H., Hasumura, S., Yashida, H., Mizutani, S., Ikenaga, H., 1998. Massive culture of human liver cancer cells in a newly developed radial flow bioreactor system: ultrafine structure of functionally enhanced hepatocarcinoma cell lines. In Vitro Cell. Dev. Biol. Anim. 34, 109–115.

Kleinman, H.K., McGarvey, M.L., Hassell, J.R., Star, V.L., Cannon, F.B., Laurie, G.W., Martin, G.R., 1986. Basement membrane complexes with biological activity. Biochemistry 25, 312–318.

Lawler, E.M., Miller, F.R., Heppner, G.H., 1983. Significance of three-dimensional growth patterns of mammary tissues in collagen gels. In Vitro 19, 600–610.

Lindenbach, B.D., Evans, M.J., Syder, A.J., Wolk, B., Tellinghuisen, T.L., Liu, C.C., Maruyama, T., Hynes, R.O., Burton, D.R., McKeating, J.A., Rice, C.M., 2005. Complete replication of hepatitis C virus in cell culture. Science 309, 623–626.

Lohmann, V., Korner, F., Koch, J., Herian, U., Theilmann, L., Bartenschlager, R., 1999. Replication of subgenomic hepatitis C virus RNAs in a hepatoma cell line. Science 285, 110–113.

Manns, M.P., McHutchison, J.G., Gordon, S.C., Rustgi, V.K., Shiffman, M., Reindollar, R., Goodman, Z.D., Koury, K., Ling, M., Albrecht, J.K., 2001. Peginterferon alfa-2b plus ribavirin compared with interferon alfa-2b plus ribavirin for initial treatment of chronic hepatitis C: a randomised trial. Lancet 358, 958–965.

Matsuura, T., Kawada, M., Hasumura, S., Nagamori, S., Obata, T., Yamaguchi, M., Hataba, Y., Tanaka, H., Shimizu, H., Unemura, Y., Nonaka, K., Iwaki, T., Kojima, S., Aizaki, H., Mizutani, S., Ikenaga, H., 1998. High density culture of immortalized liver endothelial cells in the radial-flow bioreactor in the development of an artificial liver. Int. J. Artif. Organs 21, 229–234.

Nagaya, M., Kubota, S., Suzuki, N., Tadokoro, M., Akashi, K., 2004. Evaluation of thermoreversible gelation polymer for regeneration of focal liver injury. Eur. Surg. Res. 36, 95–103.

Nakajima, N., Hijikata, M., Yoshikura, H., Shimizu, Y.K., 1996. Characterization of long-term cultures of hepatitis C virus. J. Virol. 70, 3325–3329.

Netski, D.M., Mosbruger, T., Depla, E., Maertens, G., Ray, S.C., Hamilton, R.G., Roundtree, S., Thomas, D.L., McKeating, J., Cox, A., 2005. Humoral immune response in acute hepatitis C virus infection. Clin. Infect. Dis. 41, 667–675.

Owsianka, A., Tarr, A.W., Juttla, V.S., Lavillette, D., Bartosch, B., Cosset, F.L., Ball, J.K., Patel, A.H., 2005. Monoclonal antibody AP33 defines a broadly neutralizing epitope on the hepatitis C virus E2 envelope glycoprotein. J. Virol. 79, 11095–11104.

Pietschmann, T., Lohmann, V., Rutter, G., Kurpanek, K., Bartenschlager, R., 2001. Characterization of cell lines carrying self-replicating hepatitis C virus RNAs. J. Virol. 75, 1252–1264.

Pietschmann, T., Lohmann, V., Kaul, A., Krieger, N., Rinck, G., Rutter, G., Strand, D., Bartenschlager, R., 2002. Persistent and transient replication of full-length hepatitis C virus genomes in cell culture. J. Virol. 76, 4008–4021.

Pileri, P., Uematsu, Y., Campagnoli, S., Galli, G., Falugi, F., Petracca, R., Weiner, A.J., Houghton, M., Rosa, D., Grandi, G., Abrignani, S., 1998. Binding of hepatitis C virus to CD81. Science 282, 938–941.

Rosa, D., Campagnoli, S., Moretto, C., Guenzi, E., Cousens, L., Chin, M., Dong, C., Weiner, A.J., Lau, J.Y., Choo, Q.L., Chien, D., Pileri, P., Houghton, M., Abrignani, S., 1996. A quantitative test to estimate neutralizing antibodies to the hepatitis C virus: cytofluorimetric assessment of envelope glycoprotein 2 binding to target cells. Proc. Natl. Acad. Sci. U.S.A. 93, 1759–1763.

Sasaki, M., Yamauchi, K., Nakanishi, T., Kamogawa, Y., Hayashi, N., 2003. In vitro binding of hepatitis C virus to CD81-positive and -negative human cell lines. J. Gastroenterol. Hepatol. 18, 74–79.

Schmitt, A.P., Lamb, R.A., 2004. Escaping from the cell: assembly and budding of negative-strand RNA viruses. Curr. Top. Microbiol. Immunol. 283, 145–196.

Shimizu, Y.K., Feinstone, S.M., Kohara, M., Purcell, R.H., Yoshikura, H., 1996. Hepatitis C virus: detection of intracellular virus particles by electron microscopy. Hepatology 23, 205–209.

Silini, E., Bottelli, R., Asti, M., Bruno, S., Candusso, M.E., Brambilla, S., Bono, F., Iamoni, G., Tinelli, C., Mondelli, M.U., Ideo, G., 1996. Hepatitis C virus genotypes and risk of hepatocellular carcinoma in cirrhosis: a case–control study. Gastroenterology 111, 199–205.

Suzuki, T., Omata, K., Satoh, T., Miyasaka, T., Arai, C., Maeda, M., Matsuno, T., Miyamura, T., 2005. Quantitative detection of hepatitis C virus (HCV) RNA in saliva and gingival crevicular fluid of HCV-infected patients. J. Clin. Microbiol. 43, 4413–4417.

Takimoto, T., Portner, A., 2004. Molecular mechanism of paramyxovirus budding. Virus Res. 106, 133–145.

Trestard, A., Bacq, Y., Buzelay, L., Dubois, F., Barin, F., Goudeau, A., Roingeard, P., 1998. Ultrastructural and physicochemical characterization of the hepatitis C virus recovered from the serum of an agammaglobulinemic patient. Arch. Virol. 143, 2241–2245.

Wakita, T., Pietschmann, T., Kato, T., Date, T., Miyamoto, M., Zhao, Z., Murthy, K., Habermann, A., Krausslich, H.G., Mizokami, M., Bartenschlager, R., Liang, T.J., 2005. Production of infectious hepatitis C virus in tissue culture from a cloned viral genome. Nat. Med. 11, 791–796.

Yi, M.K., Villanueva, R.A., Thomas, D., Wakita, T., Lemon, S.M., 2006. Production of infectious genotype 1a hepatitis C virus (Hutchinson strain) in cultured human hepatoma cells. Proc. Natl. Acad. Sci. U.S.A. 103, 2310–2315.

Yoshioka, H., Mikami, M., Mori, Y., Tsuchida, E., 1994. A synthetic hydrogel with thermoreversible gelation. J. Macromol. Sci. A31, 113–120.

Zhong, J., Gastaminza, P., Cheng, G., Kapadia, S., Kato, T., Burton, D.R., Wieland, S.F., Uprichard, S.L., Wakita, T., Chisari, F.V., 2005. Robust hepatitis C virus infection in vitro. Proc. Natl. Acad. Sci. U.S.A. 102, 9294–9299.

Available online at www.sciencedirect.com
SCIENCE DIRECT
ELSEVIER
Virology 351 (2006) 368–380
VIROLOGY
www.elsevier.com/locate/yviro

Induction of protective immunity against severe acute respiratory syndrome coronavirus (SARS-CoV) infection using highly attenuated recombinant vaccinia virus DIs

Koji Ishii[a], Hideki Hasegawa[b], Noriyo Nagata[b], Tetsuya Mizutani[c], Shigeru Morikawa[c], Tetsuro Suzuki[a], Fumihiro Taguchi[d], Masato Tashiro[d], Toshitada Takemori[e], Tatsuo Miyamura[a], Yasuko Tsunetsugu-Yokota[e,*]

[a] *Department of Virology II, National Institute of Infectious Diseases, Toyama, Shinjuku-ku, Tokyo 162-8640, Japan*
[b] *Department of Pathology, National Institute of Infectious Diseases, Gakuen, Musashimurayama-shi, Tokyo 208-001, Japan*
[c] *Department of Virology I, National Institute of Infectious Diseases, Gakuen, Musashimurayama-shi, Tokyo 208-001, Japan*
[d] *Department of Virology III, National Institute of Infectious Diseases, Gakuen, Musashimurayama-shi, Tokyo 208-001, Japan*
[e] *Department of Immunology, National Institute of Infectious Diseases, Toyama, Shinjuku-ku, Tokyo 162-8640, Japan*

Received 22 December 2005; returned to author for revision 9 March 2006; accepted 10 March 2006
Available online 6 May 2006

Abstract

SARS-coronavirus (SARS-CoV) has recently been identified as the causative agent of SARS. We constructed a series of recombinant DIs (rDIs), a highly attenuated vaccinia strain, expressing a gene encoding four structural proteins (E, M, N and S) of SARS-CoV individually or simultaneously. These rDIs elicited SARS-CoV-specific serum IgG antibody and T-cell responses in vaccinated mice following intranasal or subcutaneous administration. Mice that were subcutaneously vaccinated with rDIs expressing S protein with or without other structural proteins induced a high level of serum neutralizing IgG antibodies and demonstrated marked protective immunity against SARS-CoV challenge in the absence of a mucosal IgA response. These results indicate that the potent immune response elicited by subcutaneous injection of rDIs containing S is able to control mucosal infection by SARS-CoV. Thus, replication-deficient DIs constructs hold promise for the development of a safe and potent SARS vaccine.
© 2006 Elsevier Inc. All rights reserved.

Keywords: Vaccinia virus; Vaccine; SARS

Introduction

Severe acute respiratory syndrome (SARS) has become a priority for healthcare agencies around the world given its communicability, associated mortality, and the potential for pandemic spread. As of 31 July 2003, 8,098 SARS cases had been identified worldwide, resulting in 774 deaths and a mortality rate of about 9.6% (World Health Organization statistics). SARS is now known to result from infection with a novel coronavirus (SARS-CoV) (Drosten et al., 2003; Ksiazek et al., 2003; Peiris et al., 2003). Evidence that SARS-CoV is the etiologic agent of SARS follows an experimental infection of macaques (*Macaca fascicularis*), fulfilling Koch's postulates (Fouchier et al., 2003). The clinical manifestations of SARS are hardly distinct from other common respiratory viral infections, including influenza. Because influenza epidemics might occur simultaneously with the eventual re-emergence of SARS, an effective SARS vaccine is urgently required, as well as more sensitive diagnostic tests specific for SARS.

Structural characterization of SARS-CoV and characterization of its complete RNA genome (Marra et al., 2003; Rota et al., 2003; Ruan et al., 2003) have provided us with the opportunity to develop a SARS vaccine. Like other coronaviruses, SARS-CoV is a plus-stranded RNA virus with a 30-kb genome encoding replicase gene products and the 4 structural proteins; i.e., spike (S), envelope (E), membrane (M), and nucleocapsid

* Corresponding author. Fax: +81 3 5285 1150.
E-mail address: yyokota@nih.go.jp (Y. Tsunetsugu-Yokota).

0042-6822/$ - see front matter © 2006 Elsevier Inc. All rights reserved.
doi:10.1016/j.virol.2006.03.020

(N) (Marra et al., 2003; Rota et al., 2003). The S protein is thought to be involved in receptor binding, while the E protein has a role in viral assembly, the M protein is important for virus budding, and the N protein has a role in viral RNA packaging (for review, see reference (Holmes, 2003)). Recently, angiotensin-converting enzyme 2 (ACE2) has been identified as a cellular receptor for SARS-CoV (Li et al., 2003). Thus, the first step of infection likely involves binding of S protein to the ACE2 receptor. In a model of MHV infection, S protein is known to contain important virus-neutralizing epitopes that elicit neutralizing antibody responses in mice (Collins et al., 1982). Therefore, the S protein of coronavirus might be manipulated to induce immunity. However, S, M, and N proteins are also known to contribute to the host immune response (Anton et al., 1996; Jackwood and Hilt, 1995). A DNA vaccine encoding the S glycoprotein of the SARS-CoV induces T cell and neutralizing antibody responses, as well as protective immunity, in a mouse model (Yang et al., 2004). Vaccination with a plasmid expressing N protein is capable of generating strong N-specific humoral and T-cell-mediated immune responses in vaccinated C57BL/6 mice (Kim et al., 2004; Zhao et al., 2005; Zhu et al., 2004). In addition, N-specific $CD8^+$ T cells provide protective immunity against some coronaviruses (Collisson et al., 2000; Seo et al., 1997).

The DIs strain is a highly restricted host range mutant of the vaccinia virus isolated by successive 1-day egg passage of the DIE vaccinia strain, an authorized strain for smallpox vaccine and actually used in Japan until 1981. DIs does not replicate and is not pathogenic in mice, guinea pigs or rabbits. Furthermore, the DIs does not replicate in various mammalian cell lines (Tagaya et al., 1961). Recently, we established a system for foreign gene expression by inserting target genes into this strain, after which expression of (i) bacteriophage T7 polymerase, and (ii) the full-length HIV-1_{NL432} *gag* gene, was observed (Ishii et al., 2002), thus demonstrating the usefulness of this system.

In the present study, we constructed a recombinant vaccinia virus DIs expressing one or more SARS-CoV structural proteins (E, M, N, and S, or a combination of E, M, and S (E/M/S), or E, M, N and S (E/M/N/S)). These rDIs vaccines were administered to mice either subcutaneously or intranasally, and the humoral and cellular immunity against SARS-CoV in vaccinated mice were analyzed. We demonstrated here that replication-deficient DIs constructs expressing S protein alone or in combination with other components, but not N alone, elicited strong protective immune responses against SARS-CoV infection.

Results

Expression of SARS-CoV structural proteins by rDIs

The structures of transfer vectors used in this study (pDIsSARS-E, pDIsSARS-M, pDIsSARS-N, pDIsSARS-S, pDIsSARS-E/M, pDIsSARS-E/M/S and pDIsSARS-E/M/N/S) were summarized in Fig. 1. Expression of SARS-CoV N and S proteins in chick embryo fibroblast (CEF) cells infected

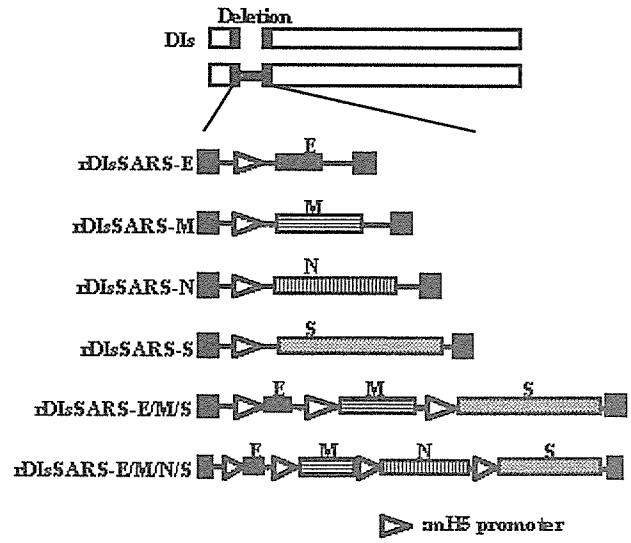

Fig. 1. Schematic diagram of rDIs constructs expressing SARS-CoV structural proteins. DNA fragments encoding E, M, N and S proteins were inserted into the location of the 15.4 kb deletion in DIs using the vaccinia virus transfer vector pDIsgptmH5. Six rDIs constructs are shown.

with rDIsSARS was detected by Western blotting using monoclonal antibodies (Fig. 2A) (Ohnishi et al., 2005). Purified SARS-CoV virion was used as a positive control (Fig. 2A, lane PC). A robust signal was detected at 50 kDa, corresponding to the N protein of SARS-CoV, as predicted by its genomic size (Marra et al., 2003; Rota et al., 2003). A band approaching 200 kDa likely corresponds to the S protein, which is known to be heavily glycosylated (Fig. 2A). Our results are consistent with data reported by Xiao et al. (2003) who expressed the full-length S glycoprotein of SARS-CoV Tor2 strain in 293 cells and demonstrated a protein approaching 180–200 kDa by SDS gel electrophoresis. Concerning the M protein, only a smear band in the stacking gel was detected using a polyclonal antibody against synthetic peptide of the M protein (Mizutani et al., 2004), presumably because it formed large oligomers with SDS-resistance in cells (Fig. 2A). Similar result was mentioned by the analysis of the M protein of SARS-CoV (Buchholz et al., 2004) and infectious bronchitis virus (Weisz et al., 1993).

The subcellular localization of S, M, and N proteins was analyzed by immunofluorescence staining. Cells infected with rDIsSARS-M demonstrated M proteins primarily co-localized with the Golgi marker GM-130 (Fig. 2B), which is consistent with the results of the recent study (Nal et al., 2005). Individually expressed SARS-CoV N protein could be detected partially with Golgi apparatus, but remained principally localized to the cytoplasm (Fig. 2B). Overexpressed recombinant SARS-S glycoprotein could be detected partially with Golgi apparatus, but also be detected throughout the cytoplasm (Fig. 2B). These results indicate that cells infected with rDIsSARS expressed significant levels of SARS-CoV proteins under the control of mH5 promoter with an expected post-translational processing (Nal et al., 2005; You et al., 2005).

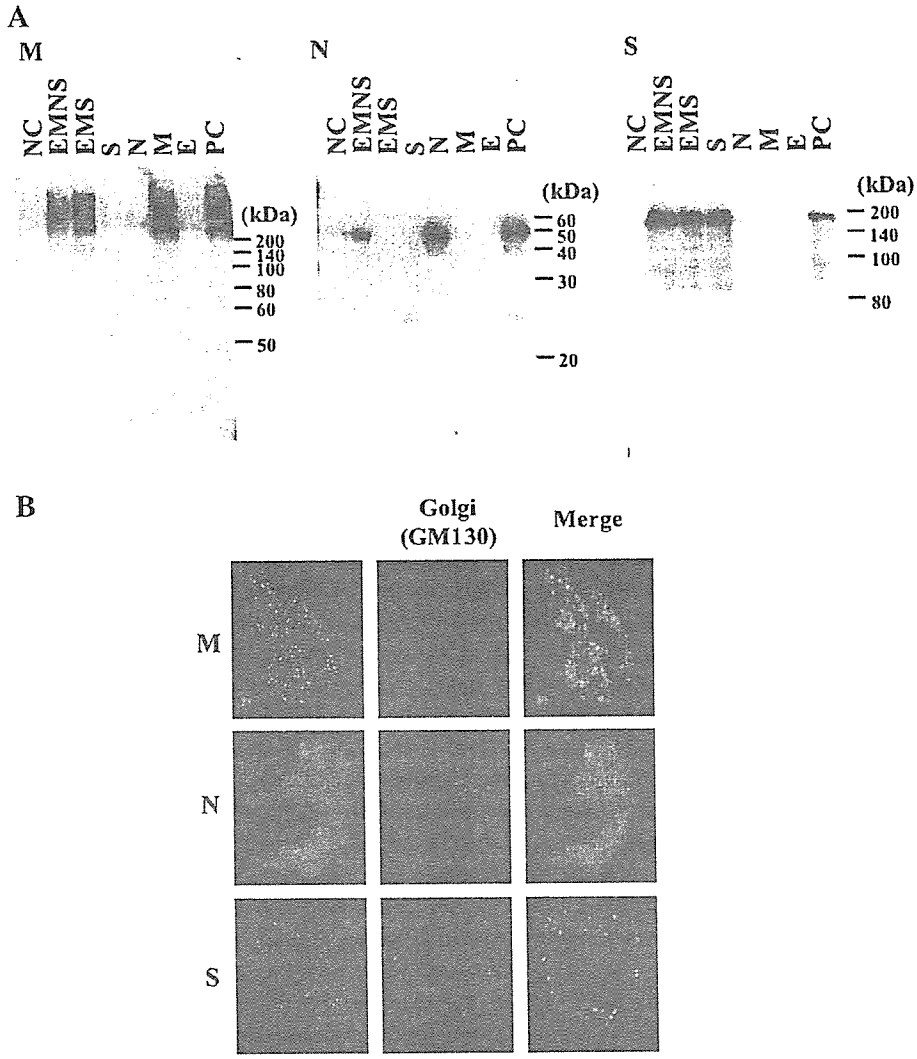

Fig. 2. Western blot analysis and indirect immunofluorescence analysis. (A) CEF cells were infected with rDIs constructs expressing SARS-CoV structural proteins (M, N and S, respectively). Purified SARS-CoV virion (0.5 μg) was used as a positive control. SARS-CoV proteins were detected using monoclonal antibodies (N and S) or polyclonal antibodies (M). Detection of bound antibodies was done with horseradish peroxidase-conjugated goat anti-mouse or anti-rabbit antibody, and visualized by chemiluminescence. (B) CEF cells were infected with rDIs constructs expressing SARS-CoV structural proteins (M, N and S, respectively). To detect SARS-CoV proteins, the cells were incubated with rabbit polyclonal antibodies against these proteins. The cells were further incubated with FITC-conjugated goat anti-rabbit IgG. To analyze subcellular localization of these proteins, monoclonal antibody against GM-130 (Golgi marker) and rhodamine-conjugated goat anti-mouse IgG were used. SARS proteins are shown in green, Golgi apparatus is shown in red and co-localization, where it occurs, is shown in yellow.

rDIsSARS induces serum IgG antibody responses specific for SARS-CoV

To examine the anti-SARS-CoV response in mice after inoculation with rDIsSARS, four mice in each group were subcutaneously or intranasally inoculated three times with 10 pfu of rDIsSARS-N, rDIsSARS-M, rDIsSARS-S, rDIsSARS-E/M/S or rDIsSARS-E/M/N/S. Ten days after the final inoculation, vaccinated mice were observed to have high levels of anti-SARS-CoV IgG antibodies in their sera (Fig. 3).

In order to prove effective vaccination, we next examined whether neutralizing antibodies against SARS-CoV were elicited in these mice. Neutralizing antibodies against SARS-CoV were induced in mice following subcutaneous or intranasal injection of rDIsSARS-S, rDIsSARS-E/M/S, or rDIsSARS-E/M/N/S, but not in mice immunized with rDIsSARS-N or rDIsSARS-M. These results of ELISA data were incorporated into Fig. 3 by depicting the neutralization positive serum as closed circles. Thus, our results, consistent with others (Bisht et al., 2004; Buchholz et al., 2004; Yang et al., 2004), indicate that the S protein is a prerequisite for eliciting a sufficient IgG antibody response for neutralization. Similar neutralizing activity was obtained in mice receiving S alone or in combination with other components. Therefore, we expected that the rDIsSARS expressing E/M/N/S proteins in combination could be the best vaccine candidate among others.

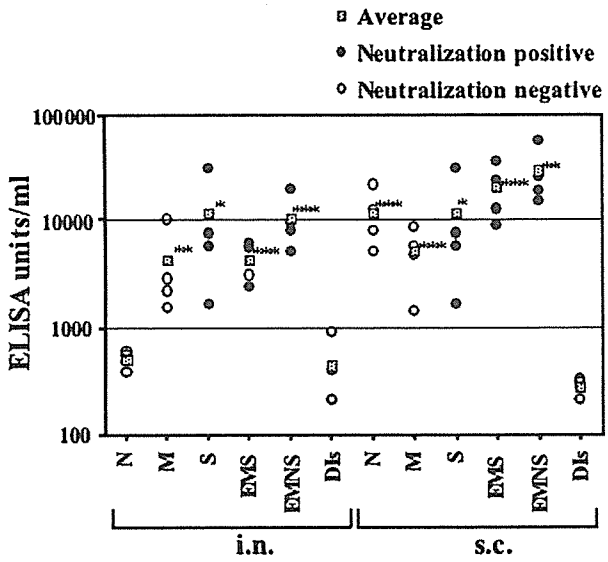

Fig. 3. Detection of anti-SARS-CoV IgG in vaccinated mice. IgG antibody levels against SARS-CoV were determined as described in Materials and methods. SARS-CoV-specific IgG titers were calculated as follows: SARS-specific IgG titer (ELISA units/ml) = (the unit value obtained for wells coated with virus-infected cell lysate) − (the unit value obtained for wells coated with non-infected cell lysate). $*P < 0.1$, $**P < 0.05$, $***P < 0.01$ vs. DIs-administered group. The data for neutralizing sera are represented by closed circles and the data for non-neutralizing sera are represented by open circles.

Intranasal inoculation of rDIsSARS expressing E/M/N/S induces SARS-CoV-specific IgA in nasal mucosa and a high level of mucosal IgG in parallel with that of serum IgG

Mucosal IgA response is believed to be crucial for the protective immunity against various pathogens (Meeusen et al., 2004). We, next, examined mucosal immunity in the respiratory tracts of mice inoculated with rDIsSARS either subcutaneously or intranasally. The level of anti-SARS-CoV IgA within nasal wash fluid of vaccinated mice was determined by enzyme-linked immunosorbent assay (ELISA). As shown in Fig. 4A, substantial levels of anti-SARS-CoV IgA were detected only in mice received intranasal inoculation of rDIsSARS-E/M/N/S, compared to those inoculated with parental DIs ($P = 0.0010$). The level of IgA detected in intranasally rDIsSARS-E/M/N/S-inoculated mice was similar to that observed following intranasal immunization with UV-inactivated, purified SARS-CoV virion (positive control). On the other hand, subcutaneous injection of all forms of rDIsSARS produced only slightly higher levels of IgA than those observed in DIs -injected control mice. Therefore, the results indicated that the subcutaneous route of injection is inefficient, especially when mucosal IgA response is required.

Since neutralizing activity was, nevertheless, detected in the nasal washes of mice following subcutaneous immunization (data not shown), we also measured anti-SARS-CoV IgG levels in the nasal washes of these mice (Fig. 4B). High levels of IgG were detected in the nasal washes of mice following nasal immunization, which were observed to correspond well with IgG levels in the serum (Fig. 4C). A similar trend was observed in mice following subcutaneous immunization, despite at a lower level than in mice immunized intranasally. These results suggest that neutralizing IgG antibodies are capable of reaching the mucosal surface if plasma levels are high enough.

Protection of rDIsSARS-immunized mice from nasal SARS-CoV challenge is achieved without mucosal IgA response

The level of protection against SARS-CoV challenge in mice following inoculation with rDIsSARS is a critical issue for the vaccine development. We inoculated three times with 10 pfu of rDIsSARS-N, rDIsSARS-E/M/S or rDIsSARS-E/M/N/S into four mice in each group either subcutaneously or intranasally. One week after final inoculation, the mice were challenged intranasally with 10^4 tissue culture 50% infectious dose ($TCID_{50}$) of SARS-CoV. The results were shown in Fig. 4D. In mice inoculated with saline, 10^3 $TCID_{50}$/ml of SARS-CoV were recovered from lung wash fluid on day 3. In contrast, titers of SARS-CoV from the lungs of mice subcutaneously immunized with rDIsSARS-E/M/S or rDIsSARS-E/M/N/S were below the limits of detection. The same was true for mice intranasally immunized with rDIsSARS-E/M/N/S, whereas the virus was recovered in mice similarly immunized with rDIsSARS-E/M/S. Taken into consideration of a relatively low or marginal level of mucosal IgA antibody in mice intranasally immunized with rDIsSARS-E/M/N/S or rDIsSARS-E/M/S, or even no IgA response by subcutaneous route as described above, it was suggested that mucosal IgG antibody, but not IgA antibody, likely contributed to the protective immunity, especially in mice simultaneously immunized with recombinant rDIsSARS-E/M/N/S.

On the other hand, titers of SARS-CoV from the lung wash fluid of mice intranasally or subcutaneously immunized with rDIsSARS-N, were similar or slightly lower than the titers of negative controls, suggesting that intranasal or subcutaneous administration of rDIsSARS-N does not protect mice from SARS-CoV challenge, which is highly reflected by the non-neutralizing nature of anti-SARS-CoV N antibodies.

Cellular immunity induced by rDIsSARS

Although now we know that the systemic neutralizing IgG antibody against SARS-CoV S protein is a major component of protective immunity, T cell responses are also important to protect hosts from various viral infection. In a previous study of coronaviruses, S protein was shown to play an important role in viral pathogenesis, as well as induction of protective immunity (Holmes, 2003). In order to assess the ability of rDIsSARS to induce SARS-CoV S-specific T cells, T cells from axillary lymph nodes (ALN), superficial cervical lymph nodes (CLN) and spleens of mice subcutaneously immunized with rDIs-SARS-S or DIs were isolated and stimulated in vitro with UV-inactivated, purified SARS-CoV virion. Culture supernatant was collected 4 days later, and the levels of interferon-γ (IFN-γ), interleukin (IL)-2, IL-4, IL-5 and tumor necrosis factor-α (TNF-α) were measured. T cells in ALN produced the greatest cytokine levels (Fig. 5, and data not shown). This is not surprising in light of the subcutaneous route of immunization.

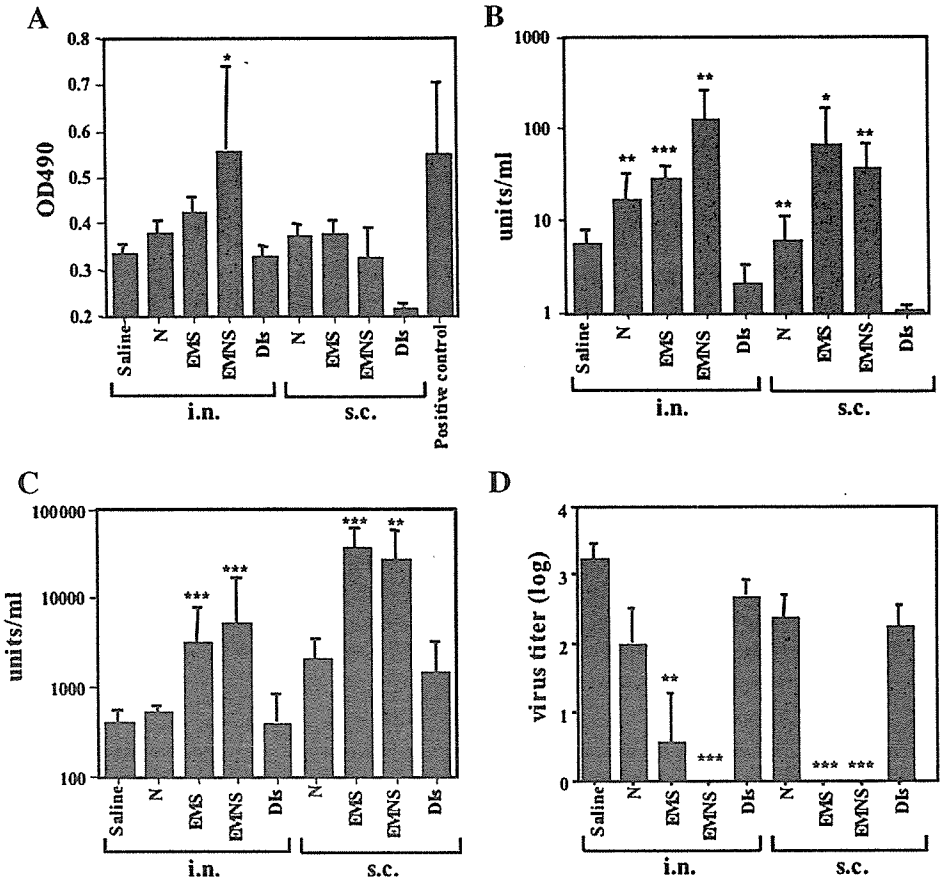

Fig. 4. Mucosally secreted anti-SARS-CoV IgG, but not IgA, antibodies are protective from nasal SARS-CoV challenge in vaccinated mice. The levels of Ig A and IgG antibodies against SARS-CoV were determined as described in Materials and methods. (A) Titers of anti-SARS-CoV IgA in the nasal washings of vaccinated mice. Error bars represent the mean ± SD. (B) Titers of anti-SARS-CoV IgG in the nasal washings of vaccinated mice. Error bars represent the mean ± SD. (C) Titers of anti-SARS-CoV IgG in the sera of vaccinated mice. Error bars represent the mean ± SD. (D) The titers of SARS-CoV in the lungs of vaccinated mice challenged 1 week later with 10^4 $TCID_{50}$ of SARS-CoV. Virus titers are expressed as $\log_{10}TCID_{50}$. Error bars represent the mean ± SD. $*P < 0.1$, $**P < 0.05$, $***P < 0.01$ vs. DIs-administered group.

Notably, mice immunized with rDIsSARS-S produced a high level of IFN-γ upon in vitro stimulation with UV-inactivated, purified SARS-CoV virion. The production of TNF-α, an inflammatory cytokine, was significantly elevated in T cells in ALN of rDIsSARS-S immunized mice after in vitro stimulation with virion antigens. However, TNF-α production was observed also in mice immunized with parental DIs without in vitro stimulation with virion antigens. Since T cells from the

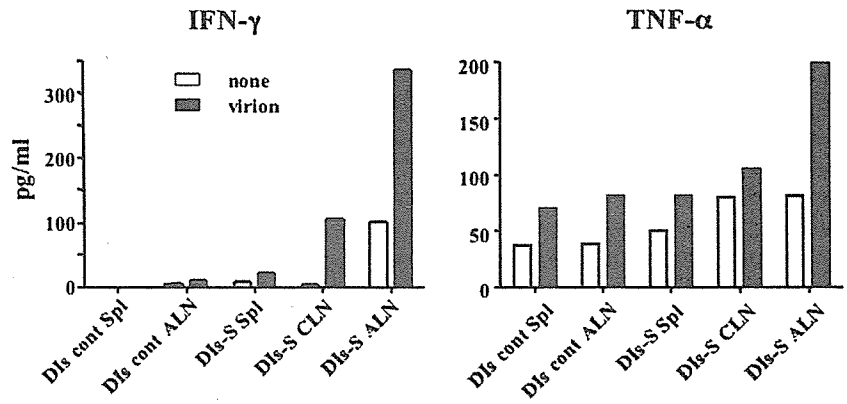

Fig. 5. In vitro response of SARS-CoV-specific T cells in mice subcutaneously immunized with rDIsSARS-S. CLN, ALN and spleens were obtained from mice 1 week after the third vaccination of either DIs control or rDIsSARS-S. After preparation of single cell suspensions, T cells were purified and cultivated with irradiated and T-cell depleted normal BALB/c mouse splenocytes as APCs in the presence or absence of 10 μg/ml of purified UV-irradiated SARS-CoV virion. Four days later, IFN-γ and TNF-α concentrations in the culture supernatant were measured.

lymph nodes of naïve mice did not produce cytokines even after in vitro stimulation with virion antigens (data not shown), it is possible that injection of DIs induces mild local inflammation, even when viral proliferation does not occur at the injection site. The pattern of IL-2, IL-5 and IL-4 production were similar to that of IFN-γ, and the maximum level of these cytokines in ALN T cells from rDIsSARS-S-immunized mice were 254, 227 and 88 ng/ml, respectively.

Next, we analyzed the antigenic epitopes of SARS-CoV-specific T cells in the spleen. We carried out IFN-γ enzyme-linked immunospot (ELISPOT) analysis using four 20-mer peptides corresponding to the ACE2 binding region of the S protein selected using the SYFPEITHI score (S44-47), as well as overlapping 20-mer peptides pool covering a whole N protein. When the splenic T cells of mice were analyzed following intranasal or subcutaneous immunization with the most potent vaccine, rDIsSARS-E/M/N/S, a high level of reactivity against S46 was observed especially in the T cells of subcutaneously immunized mice (Fig. 6A). Zhi et al. recently identified a $CD4^+$ T cell epitope, known as NYNYKYRYL, in BALB/c mice (Zhi et al., 2005). S46 contains this sequence, thus, these IFN-γ-producing T cells are likely $CD4^+$ T cells. To detect N-specific T cells, mice subcutaneously or intranasally immunized with rDIsSARS-N were analyzed by ELISPOT. In this case, ten peptides were pooled from amino-terminus of N protein, resulting in 5 pools of peptides. We thus detected N-reactive T cells capable of recognizing the first 10 peptides pool (Fig. 6B), and observed a greater proportion of N-specific T cells following nasal immunization than subcutaneous immunization. These results indicate that S- and N-specific T cells are generated systemically by rDIs.

In order to elucidate whether or not SARS-CoV-specific $CD8^+$ T cells were induced by immunization with the rDIs, the splenic T cells of mice subcutaneously or intranasally immunized with rDIsSARS-E/M/N/S were further analyzed by ELISPOT using a stably S-expressing A20.2J B cell S6.2 clone, as an antigen presenting cells (APC). Expression of S protein on the S6.2 clone was confirmed by FACS analysis using anti-SARS S monoclonal antibody (Fig. 7A). An empty vector transfectant, BOS-5, was used as a negative control APC. Subcutaneous and intranasal immunization with the most potent rDIsSARS-E/M/N/S generated a significant level of S-specific T cells (Fig. 7B), and a dramatic decrease in S-specific T cells was observed following partial depletion of $CD8^+$ T cells (Fig. 7C). Therefore, rDIsSARS-E/M/N/S was able to induce both SARS-CoV-reactive $CD4^+$ and $CD8^+$ T cells.

Histopathological findings

The immunogenicity of rDIs expressing SARS-CoV structural proteins was further evaluated by histopathological and immunohistochemical analysis of lung tissue in mice, the primary infection site of SARS-CoV (Fig. 8). Slight migration of inflammatory cells and mild disruption of the bronchial epithelium were detected in lung tissue of mock-vaccinated mice. SARS-CoV antigens were diffusely observed within the bronchial and alveolar epithelium. In contrast, significant lymphocytic infiltration into peribronchial sites, with little to no detection of SARS-CoV antigens, was observed in mice intranasally immunized with rDIsSARS-E/M/S or rDIsSARS-E/M/N/S (Fig. 8). The infiltrating lymphocytes were found to be CD3-positive T-cells, as determined by immunohistochemistry with anti-CD3 antibody (Fig. 8). On the other hand, intranasal or subcutaneous immunization by only N-expressing DIs induced neither T-cell infiltration nor protective immunity against SARS-CoV, despite of the induction of N-specific antibodies and T cells. These results suggest that marked induction of T-cell response in mice immunized with rDIs-SARS-E/M/S and rDIsSARS-E/M/N/S help to eliminate SARS-CoV from the lung tissue. On the other hand, intranasal or subcutaneous immunization by only N-expressing DIs did not induce protective immunity against SARS-CoV, despite of the

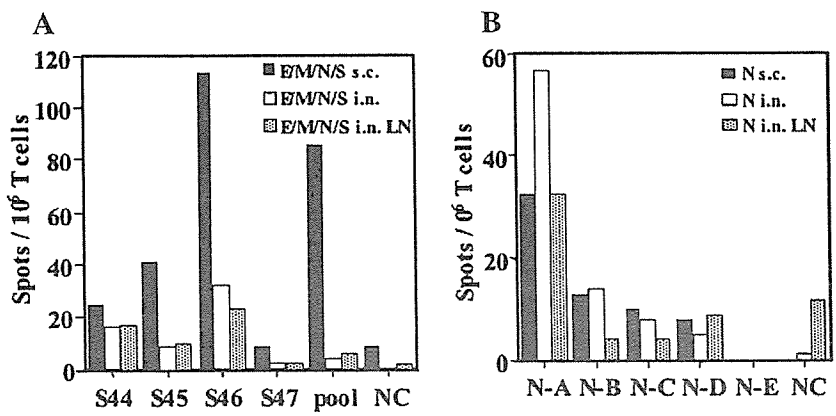

Fig. 6. Detection of SARS-CoV-specific T cells elicited by rDIsSARS-E/M/N/S or rDIsSARS-N vaccination. Splenic and lymph node (LN) T cells of mice s.c. or i.n. immunized with recombinant rDIsSARS-E/M/N/S (A) or rDIsSARS-N (B) were separated using a MACS system (Miltenyi Biotec), and IFN-γ ELISPOT analysis was performed. (A) T cells (5×10^5 cells) from mice immunized with rDIsSARS-E/M/N/S were cultured with irradiated A20.2J B cells (1×10^4), in triplicate, in a 96-well membrane plates coated with IFN-γ capture antibody in the absence or presence of 5 μM of S peptides (S44–S47). The numbers of IFN-γ spot-forming cells were then counted and are depicted. (B) T cells from mice immunized with rDIsSARS-N and A20.2J B cells were cultured as described in A. N protein (422 amino acids) was divided into 5 parts by 100 amino acids (A, B, C, D and E) and 10 peptides each of pooled 20-mer overlapping peptides specific to the each stretch of N sequence were used as an antigen.

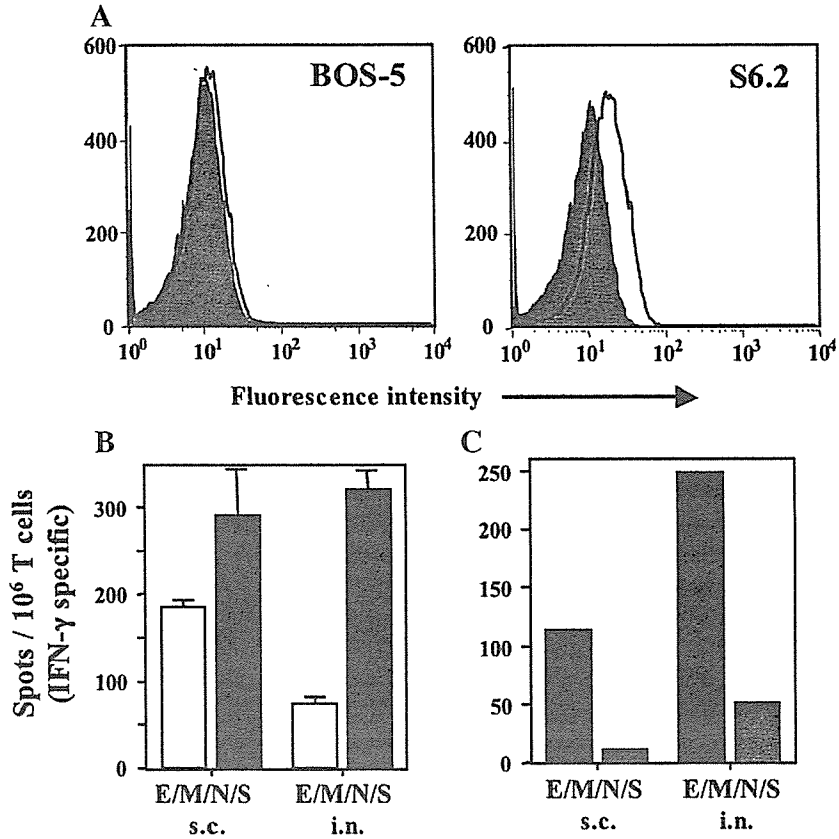

Fig. 7. Detection of SARS-CoV S-specific $CD8^+$ T cells in mice immunized with rDIsSARS-E/M/N/S. (A) A20.2J B cell clone expressing S (S6.2) or empty vector (BOS-5) was stained with biotinylated anti-SARS-CoV S monoclonal antibody (solid line) or control IgG (shadowed line), followed by the incubation with streptavidin-APC, and then analyzed by FACScalibur. A histogram of APC fluorescence of gated live cells (PI negative) is depicted. (B) Splenic T cells from mice immunized s.c. or i.n. with recombinant rDIsSARS-E/M/N/S were purified and IFN-γ ELISPOT analysis was carried out using γ-irradiated S6.2 and BOS-5 as APCs. The number of T cells reactive for BOS-5 control (white column) and S6.2 (black column) cells are shown. Error bars represent the mean ± SD. (C) Using the same splenic T cells as in panel B, $CD8^+$ T cells were partially removed using anti-CD8 mAb-coated magnetic beads (Miltenyi Biotec), and the number of T cells reactive for BOS-5 and S6.2 cells were counted by ELISPOT. The number of BOS-5-reactive T cells was subtracted and the number of S-specific T cells is depicted. Black columns: total T cells; grey columns: partially CD8-depleted T cells.

induction of N-specific antibodies and T cells. Thus, rDIs expressing the S protein, along with other membrane components (E/M and E/M/N), are capable of inducing strong immunity of both humoral and cellular arms and are fully competent to clear SARS-CoV infection.

Discussion

The DIs strain, which replicates well in CEF cells but not in most mammalian cells, was isolated from the DIE strain of the vaccinia virus during serial 1-day egg passage, and it is characterized by the induction of tiny pocks on chicken chorioallantoic membrane (Tagaya et al., 1961; Kitamura et al., 1967; Ishii et al., 2002). The DIs-derived recombinant viruses express high levels of viral and inserted genes, even in non-permissive cell lines without any cytopathic effects (Ishii et al., 2002). In earlier studies, MVA strain of vaccinia virus, which is also replication-incompetent in most mammal cells, was used to express a variety of foreign genes and some of these recombinant viruses were studied as candidate vaccine vectors and appeared to be more effective than many replication-competent vaccinia virus vaccines (Sutter and Moss, 1992; Sutter et al., 1994; Belyakov et al., 1998; Nam et al., 1999; Stittelaar et al., 2000). rDIs does not replicate nor produce infectious virions in most mammalian cells, therefore the DIs strain has a safety advantage when used as a recombinant vaccine vector as for MVA. Recently, a recombinant DIs, rDIsSIVGag, expressing a full-length *gag* gene of SIV, was developed, and demonstrated to have a potential for use as an HIV/AIDS vaccine (Someya et al., 2004).

Attempts at vaccine development against SARS-CoV are ongoing by a number of organizations using various techniques (see review, (Groneberg et al., 2005)). DNA vaccines (Kim et al., 2004; Yang et al., 2004; Zhu et al., 2004; Zhao et al., 2005) and viral vectors such as vaccinia virus (Bisht et al., 2004; Weingartl et al., 2004), parainfluenza virus (Bukreyev et al., 2004), adenovirus (Zakhartchouk et al., 2005) and rhabdoviruses (Faber et al., 2005; Kapadia et al., 2005) are used as recombinant vaccines. Yang et al. (2004) showed that viral replication was reduced by more than six orders of magnitude in the lungs of mice vaccinated with these S plasmid DNA expression vectors, and protection was mediated by a humoral but not a T-cell-dependent immune mechanism. Bisht et al. (2004) showed that inoculation of BALB/c mice with a